Additive Manufacturing 77 (2023) 103806

Contents lists available at ScienceDirect

Additive Manufacturing

journal homepage: www.elsevier.com/locate/addma

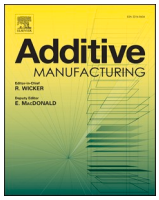

Research Paper

3D-printed polylactide composites reinforced with short lyocell fibres – Enhanced mechanical properties based on bio-inspired fibre fibrillation and post-print annealing

Christian Gauss [a,*], Kim L. Pickering [a], Nina Graupner [b], Jörg Müssig [b]

[a] School of Engineering, The University of Waikato, Private Bag 3105, Hamilton, New Zealand
[b] The Biological Materials Group, Department of Biomimetics, HSB - City University of Applied Sciences, Neustadtswall 30, D-28199 Bremen, Germany

ARTICLE INFO

Keywords:
Bio-composite
Additive manufacturing
Regenerated cellulose
Fibre modification

ABSTRACT

In this study, 3D printable polylactide (PLA) composites reinforced with 10, 20 and 30 mass% of short lyocell fibres were produced by melt compounding PLA modified with maleic anhydride. Based on bio-inspired anchoring systems, fibrillated fibres were also employed in 30 mass% fibre composites. The resulting 3D printed samples displayed outstanding mechanical performance, particularly with high fibre content. Compared to neat PLA, unmodified formulations showed reduced tensile strength and strain at break with the addition of fibres, but they had a moderate improvement in Young's modulus. However, by combining fibre fibrillation, matrix modification, and post-printing annealing, we achieved an excellent balance of tensile strength (85 MPa), Young's modulus (7.2 GPa), and strain at break (3.2%) - the highest reported values for such composites. Incorporating fibres and increasing PLA crystallinity via heat treatment significantly enhanced the thermomechanical stability of the composites, raising the storage modulus up to 38 times at 60 °C and 200 times at 80 °C compared to neat PLA. This combined strategy paves the way for the 3D printing of high-performance structures using 100% bio-derived materials.

1. Introduction

There is a growing interest in developing and using biobased composites made of bioderived polymers and fibres as substitutes for synthetic and petroleum-based composites as they can be used to improve the sustainability and circularity of materials [1]. One of the main advantages of biobased composites is the variety of fibres that can be used to reinforce the matrix and their suitability for different manufacturing processes, including injection moulding [2–4], compression moulding [5–7], and additive manufacturing [8–11]. Cellulose-based fibres, such as hemp, bamboo, flax, harakeke, wood fibres, and other sources in the form of micro or nano fibres, have been explored as reinforcing elements for 100% bio-derived composites [12–16]. Lyocell fibres, one type of regenerated cellulose fibre, are mainly used in the textile industry for the production of clothing, bed linen, pillows, denim, towels, carpets, technical textiles, hygiene products and others [17], but have also demonstrated great potential as a bio-derived fibre to reinforce composites made of petroleum-based thermoplastic polymers such as polypropylene (PP) [18–21] and polyethylene (PE) [22], and bio-derived and biodegradable thermoplastics such as polylactide (PLA) [10,23–26] and polyhydroxybutyrate (PHB) [27]. These fibres are generally derived from wood pulp and produced by an eco-friendly lyocell process that uses N-methyl morpholine-N-oxide (NMMO) to dissolve cellulose that is later regenerated in water forming fibres with uniform properties and interesting mechanical properties, including high strength and high strain at break [28,29]. The lyocell fibres have similar physical properties to cotton, but they have better mechanical properties and different cellulose crystal structure; lyocell has a cellulose II structure [30] whereas the native cellulose in cotton and other plant fibres have a cellulose I structure (with a higher proportion of Iβ) [31]. Lyocell in the form of short fibres [10,18,22,24,27,32], fleeces or felts [7,33,34], and fabrics [25,35,36] have been explored in the manufacturing of biobased composites to assess the effect of different fibre content, fibre fineness, fibre length, and fibre orientation on the mechanical performance of the biocomposites.

The hydrophilic nature of cellulose fibres and the hydrophobicity of most thermoplastics directly influence the adhesion between fibre and polymer. Matrix modification and/or surface treatment of the fibres are

* Corresponding author.
E-mail address: cgauss@waikato.ac.nz (C. Gauss).

https://doi.org/10.1016/j.addma.2023.103806
Received 28 May 2023; Received in revised form 23 August 2023; Accepted 2 October 2023
Available online 5 October 2023

generally recommended to obtain optimum mechanical and physical properties, especially if short fibres are used. Incorporating coupling agents is one of the most common methods to improve the interface between fibre and matrix, resulting in better tensile strength, stiffness, and impact resistance of biobased composites [1]. Maleic anhydride-grafted PP (MAPP), for example, has been used in PP-based composites reinforced with lyocell and natural fibres to create a "bridge" between the hydrophobic matrix and hydrophilic fibres [37,38]. A similar approach has been used to improve the fibre/matrix interface in PLA-based composites, using maleic anhydride (MA) to modify the matrix "in situ" during the compounding process with the fibres [39–41]. The modification of the fibre surface is another possibility to improve the fibre/matrix interface. A wide range of strategies have been explored to modify the fibre surface to improve adhesion, e.g., by chemical treatments such as alkali and silane treatment [42,43], grafting [15,44], plasma treatment [35,45], and selective fibre fibrillation [9,21,46,47]. Considering the smooth surface of lyocell fibres, which results in poor apparent fibre/matrix interfacial adhesion, fibre fibrillation can be used to increase the surface area and the bonding surface. Although the fibrillation of lyocell fibres is well understood, only a few studies reported the use of fibrillated lyocell fibres as reinforcement of composites [21,46,48]. Using short untreated and fibrillated fibres with random orientation, Cheng et al. produced PP and PVA matrix composites with a maximum fibre fraction of 10 mass%, obtaining higher strength and Young's moduli in both matrices when fibrillated fibres are used. More recently, Graupner et al. demonstrated that fibre fibrillation enhanced the apparent interfacial shear strength of the lyocell fibre in PLA and PP matrices and improved Young's modulus, tensile strength, and impact strength of composites reinforced with a fibre volume fraction of 30%. In the case of PLA, the tensile strength and Young's modulus were improved by a factor of 1.62 and 1.20, respectively, in relation to the composites with unmodified fibres [48]. The fibrillation tendency of lyocell fibres is explained by the low lateral intermolecular forces among the elementary fibrils because of their isolated and intact cellulose crystallites and their high affinity for alkali and water retention [49,50]. The outer crystalline regions of the fibres break and separates longitudinally from the fibres during fibrillation, leading to partial detachment of the fibrils from the main fibre [51].

Additive manufacturing, or three-dimensional (3D) printing, is a powerful manufacturing method that opens new opportunities to develop and design structures using bioderived polymers and composites. Material extrusion methods, in special fused deposition modelling (FDM), also known as fused filament fabrication (FFF), is one of the most used methods for 3D printing using polymers or polymeric composites due to its simplicity and low cost of operation [8]. Different natural fibres have been used to reinforce composites for FDM, including wood fibres [52,53], hemp [13,54], bamboo [53], flax [55], harakeke [9], lyocell [10], and nanofibrillated cellulose [16,44] with fibre content varying between 1 and 30 mass%. These 3D-printed composites presented tensile strengths between 28 and 80 MPa and Young's moduli between 2 and 7 GPa, depending on the fibre content and printing orientation. In most studies, a considerable decrease in the strain at break and sometimes in the tensile strength is reported when higher fibre loading is used (above 20 mass%). Three main issues cause these problems; the poor interface between fibre and matrix (chemistry related), the difficulty in getting proper dispersion of the fibres in the composites (process and chemistry-related), and printing defects. However, as in conventional manufacturing methods, it has been shown that modifying the surface of the fibres, either chemically or physically, can positively affect the processability and mechanical properties of PLA-based composites used in 3D printing [9,44,56,57]. In addition, post-printing treatments, such as heat treatment, can also be used to increase the crystallinity of PLA and improve the thermo-mechanical and creep performance of reinforced composites [10,44,58,59].

Although there are many works on the use of bio-derived fibres to reinforce PLA-based composites for FDM, the resulting improvement of the mechanical properties is limited. These hurdles have hindered the widespread use of PLA-based composites reinforced with bio-derived fibres for applications where mechanical performance and thermo-mechanical stability are critical. Lyocell fibres have demonstrated great potential as reinforcement in PLA-based composites produced by traditional manufacturing methods, improving not only strength and stiffness but also, in many cases, strain at break and impact toughness [60–66]. In addition, the uniform dimensions and mechanical properties of the fibres, renewability as well as their tendency to fibrillate and thus create a larger specific fibre surface area make lyocell fibres an interesting option for 3D printing applications in comparison to natural fibres. In this work, a new approach to produce PLA-based composites reinforced with short bio-derived fibres for 3D printing was developed to solve two main issues: poor interfacial bonding between fibre and matrix and the poor thermo-mechanical stability of PLA.

Plant root systems have a large specific surface area due to their many fine and branched roots and exhibit efficient soil anchoring. This principle of surface enlargement was used as a model for improving fibre-matrix bonding in cellulose fibre-reinforced composites. By using a combination of fibre surface fibrillation and matrix modification, thermoplastic wires (referred to as "filament" in the 3D printing sector) with good printability and mechanical performance were produced. Samples 3D printed by FDM were characterised by tensile testing, thermo-mechanical analysis and microstructural investigation. Besides fibre and matrix modification, post-printing annealing was also explored as a strategy to improve the mechanical and thermo-mechanical properties of the composites.

2. Materials and methods

2.1. Materials

Polylactide (PLA) grade 2003D with melt flow index (MFI) of 6 g/10 min (210 °C, 2.16 kg) and specific gravity of 1.24 g/cm^3 was purchased from NatureWorks®. Lyocell fibres (FCP400) with a nominal length of 400 μm were supplied by Lenzing®, Austria. The fibres have a nominal linear density of 1.3 dtex (equivalent to diameters between 10 and 12 μm). Optical microscopy images of the fibres are given in Fig. 1. Dichloromethane (DCM) (Merck Millipore ≥ 99.5%, Sigma-Aldrich, NZ) was used for the fibre extraction. Maleic anhydride (MA) (95%, Sigma-Aldrich, NZ) and dicumyl peroxide (DCP) (98%, Sigma-Aldrich, NZ) were used for PLA modification. Isohexane (Rotisolv(R) ≥ 98%, Carl Roth GmbH + Co. KG, DE) and acetone (≥ 99.5%, Carl Roth GmbH + Co. KG, DE) were used in the fibre fibrillation process.

2.2. Fibre fibrillation

The fibrillation of the lyocell fibres was carried out using different solvents in an ultrasonic bath with a volume of 2.2 L, a working quantity of 1.4 L, an operating frequency of 40 kHz and an ultrasonic power of 120 W (Emmi-H22, EMAG AG, Mörfelden-Walldorf, DE). First, 30 g fibres were placed in the ultrasonic bath with demineralised water for 30 min. Then, the water was replaced with isohexane and the fibres were soaked for 60 min. Afterwards, isohexane was replaced with acetone and the fibres were treated for 60 min. In a final step, the fibres were placed again in demineralised water in the ultrasonic bath for 15 min and were finally air-dried for a few days. The described procedure was repeated one more time to obtain approx. 60 g of fibrillated fibres.

2.3. 3D printing filaments production

The composites were produced by melt compounding PLA with the lyocell fibres, followed by extrusion to produce the 3D printing filaments, following a similar procedure reported in [9]. First, the fibres were melt compounded with neat PLA using a custom-made Sigma

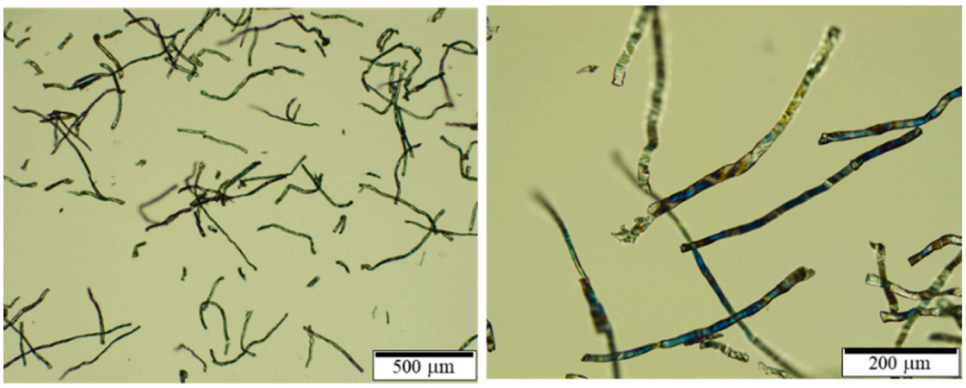

Fig. 1. Optical microscopy images of as-received lyocell fibres.

blade-type compounder for 10 min (until the measured torque became constant) according to the composition shown in Table 1. The formulations using fibrillated fibres are identified with "-fib" in the sample ID. The compounding temperature (between 180 and 195 °C) had to be increased in some formulations because of the torque limitations of the melt compounder. In this process, batches of 60 g were used, and PLA was first melted and mixed for approximately 3 min before adding the fibres. Maleic anhydride (MA) was used to modify the PLA matrix to improve the compatibility with the fibres through an in-situ modification, following similar methodologies reported in [39–41]. In these formulations, 2 mass% of MA in relation to PLA was added to the melt compounder after PLA was completely melted. The catalyst dicumyl peroxide (DCP), 10 mass% in relation to MA, was also added with MA during compounding. After adding MA and DCP, the PLA-MA was mixed for 3 min before adding the fibres, as conducted for the other formulations. After compounding, the composites were granulated into particles of < 4 mm using a Moretto GR knife mill (Mercer County, PA, USA). The particles were vacuum dried at 60 °C for 4 h and extruded into filaments using a Filabot EX2 single screw extruder (Barre, VT, USA) at 180–185 °C. An air cooling system was used to cool the filament. The extrusion and pooling speeds were adjusted to produce filaments with a constant diameter of 1.70 ± 0.1 mm. Images of the filaments were taken using a SZX7 Olympus stereo microscope (Tokyo, Japan).

2.4. 3D printing

Samples for tensile testing, dynamic mechanical analysis (DMA), and X-ray diffraction (XRD) analysis were 3D printed in a MakerGear™ M2 desktop 3D printer (Beachwood, OH, USA) using the Simplify 3D® software package for slicing the CAD files and controlling the 3D printer. Before printing, all the filaments were vacuum dried at 50 °C for 2 h. The samples were printed using the printing parameters given in Table 2. All the samples were printed using a perimeter (shell) of one printing line (approximately 0.75 mm). After 3D printing, one set of samples for each formulation (tensile and DMA specimens) was heat treated at 105 ± 2 °C for 2 h in a laboratory oven. All the samples were conditioned in a climatic chamber (Binder GmbH, Model KMF 115, Tuttlingen, DE) for 48 h at 23 °C and 50% relative humidity before testing. For one of the formulations (with 30 mass% of fibrillated fibre), an additional set of samples was printed to assess the influence of the infill raster angle on the mechanical properties. In this case, samples were printed using two different infill raster angles: 90° and alternate layers of 0/90°. A perimeter shell of one printing line was used. In order to reduce the influence of the perimeter line on the mechanical properties, the width of the sample shown in Fig. 2a was increased by 20%. Controls were printed using neat PLA.

Table 2
Parameters used for the 3D printed samples.

Parameter	Value
Infill density	100%
Nozzle diameter	0.75 mm
Raster angle	0 ° (for all the layers)
Bed temperature	70 °C
Nozzle temperature	210 °C
Printing speed	1800 mm/min
Layer height	0.1 mm

2.5. Materials characterisation

2.5.1. Tensile testing

Tensile testing of the 3D printed samples was conducted on an Instron® 5982 universal testing machine (Norwood, MA, USA) equipped with a 5 kN loadcell. The samples were printed using ASTM D638 type V samples, with free-span nominal dimensions of 3.18 mm, 1.20 mm and 10.96 mm for width, thickness, and length, respectively (Fig. 2a). All the samples were tested at a crosshead displacement rate of 2 mm/min. A clip-on extensometer of 10 mm was used to measure the tensile strain. Five specimens per condition were tested, and only specimens fractured within the free span were considered valid.

Table 1
Compositions of the formulations used for the production of PLA/lyocell composites.

Formulation ID	Fibre content in mass%	PLA content in mass%	Maleic anhydride content in mass%	Compounding temperature in°C	Extrusion temperature in°C
PLA	0	100.0	-	180	180
PLA-MA	0	98.0	2.0	180	180
L10	10	90.0	-	180	185
L10-MA	10	88.2	1.8	180	185
L20	20	80.0	-	195	185
L20-MA	20	78.4	1.6	190	185
L30	30	70.0	-	195	185
L30-MA	30	68.6	1.4	190	185
L30Fib	30	70.0	-	195	185
L30Fib-MA	30	68.6	1.4	190	185

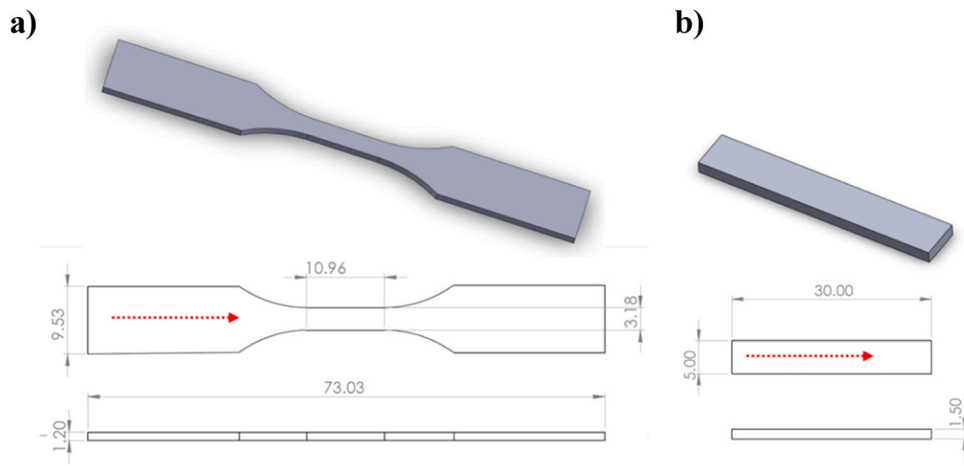

Fig. 2. Dimensions of 3D-printed samples for tensile tests (a) and dynamic mechanical analysis (b). The red arrows indicate the printing direction.

2.5.2. Differential scanning calorimetry (DSC)

The 3D-printed samples were characterised through DSC analysis. Small samples of 6–10 mg were extracted from the specimens and analysed in a Netzsch DSC3500 Sirius differential scanning calorimeter (Selb, DE) using aluminium crucibles from 20° to 200°C at 10 °C/min with a nitrogen flow of 60 mL/min. The obtained scans were used to determine glass transition (T_g), melting (T_m), and cold crystallisation (T_{cc}) temperatures. The PLA crystallinity of the samples was determined according to Eq. (1) [67]:

$$X_c = \frac{(\Delta H_m - \Delta H_{cc})}{\Delta H_f \times X_{PLA}}.100 \quad (1)$$

where ΔH_m and ΔH_c are the enthalpies of melting and cold crystallisation, respectively, ΔH_f is the melting enthalpy of 100% crystalline PLA (93 J/g) [67], and X_{PLA} is the mass fraction of PLA in the composite.

2.5.3. Microstructural analysis

Unmodified and fibrillated fibres and fractured samples of the 3D printed samples were analysed by scanning electron microscopy (SEM) in a Hitachi Regulus 8230 SEM (Hitachinaka, Japan) at 3 kV using a secondary electrons detector. Before the analysis, the samples were metallised with 5 nm of platinum in a Quorum Q150V plus (Laughton, East Sussex, UK).

2.5.4. Fibre extraction and analysis

In order to evaluate the effect of filament processing and printing on the fibre length, the fibres were extracted from the 3D printed samples (from the conditions with 30 mass% of fibre) by dissolving PLA in dichloromethane (DCM) followed by filtration. Samples extracted from 3D-printed tensile test samples were dissolved at room temperature in DCM under continuous stirring at a concentration of 10 g/L for 6 h. The solution was then vacuum filtered using paper filters, and the obtained fibres were rinsed thrice with DCM and dried at room temperature for 48 h. The fibres before processing (as-received and fibrillated) and extracted fibres were analysed with the image analysis software FibreShape (X-Shape, version 6.1.4; IST AG, Vilters, CH). The fibres were manually prepared on a glass slide with a size of 40 × 40 mm^2 and a thickness of 2 mm. Afterwards, the glass slide with the prepared fibres was covered with a second glass slide, fixed with adhesive tape at the edges, and scanned with a Canoscan scanner CS 4000 (Canon, New York, USA) at a resolution of 4000 dpi in transmitted light mode. For the analysis, a measuring mask for 4000 dpi resolution and no additional calibration was used. More than 3200 fibres were measured per test series.

2.5.5. X-ray diffraction (XRD) – fibre orientation

The fibre orientation on the printed composites was assessed by XRD analysis, following a similar methodology used in [10,44]. A sample in the shape of a disk with a diameter of 30 mm and thickness of 1.5 mm was 3D printed with the L30Fib-MA formulation using raster angles of 0 ^{o} (all the layers). A control made of as-received lyocell fibres with random orientation was also prepared for XRD analysis. The control was produced by pressing (5 tons) the lyocell fibres into a circular "mat" with a diameter of 30 mm using a manual hydraulic press. The samples were analysed in a Panalytical Empyrean XRD (Worcestershire, UK) in transmission mode using CuKα radiation (40 kV; 40 mA) and a PixCel linear detector. The samples were first analysed in a continuous 2θ scan mode between 5° and 45° 2θ using a scanning step of 0.01° and exposure time of 40 s at φ angles (disc rotation axis) of 0° and 90°. Then, a scan through the φ axis (0–180 ^{o}) was conducted at the 2θ angle of approximately 21.4°, which is the diffraction of the plane (020) of cellulose II, using a step size of 0.5° and exposure time of 10 s

2.5.6. Dynamic mechanical analysis (DMA)

Dynamic thermomechanical analyses were conducted in a Perkin Elmer DMA8000 (Waltham, MA, USA) using a single cantilever mode. Samples of 5 × 1.5 × 30 mm^3 (Fig. 2b) were 3D printed using the printing parameters given in Table 2. All the samples were tested using a frequency of 1 Hz and dynamic displacement of 0.05 mm from 25 to 140 °C.

2.5.7. Statistics

The mechanical testing results are presented with the corresponding arithmetic averages (Avg.) and coefficient of variation (COV). The data was analysed in the statistical software Minitab® 18 using a one-way analysis of variance (ANOVA) test and the significant differences among averages were calculated using Tukey's method with 95% of confidence. The statistical analysis results are indicated as an upper letter in each average. Different letters mean that there is a significant statistical difference.

3. Results and discussion

3.1. 3D printing of lyocell/PLA composites

Stereo optical microscopy images of the composite in the form of filaments with 10–30 mass% of fibre content are shown in Fig. 3a. Independently of the fibre content, the filaments based on PLA only and PLA-MA present similar surface roughness. However, the filament with 30 mass% of fibre in PLA (L30) presented a more pronounced brown colour, which is attributed to the higher temperature necessary in the

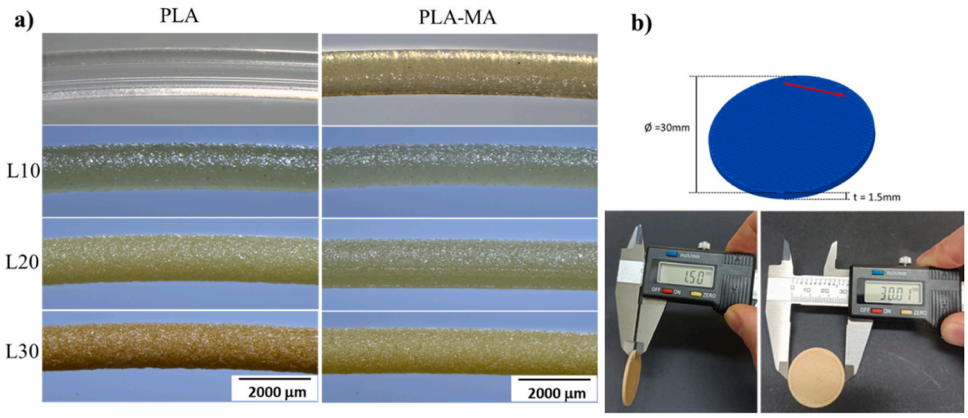

Fig. 3. 3D printing filaments with 10–30 mass% of lyocell fibres in the PLA and PLA-MA matrices (a) and a 3D printed object using a formulation with 30 mass% of fibres (b).

compounding process for this formulation. Although the onset temperature of degradation of lyocell fibres is approximately 313 °C (see Table S2), the high permanence time (about 10 min) during the compounding process could have triggered early stages of thermal degradation in the fibres. Nonetheless, the temperatures involved in the compounding and filament production processes (180–195 °C) and 3D printing (210 °C) are much lower than the degradation temperatures for the filaments with high fibre content. According to thermogravimetric analyses (TGA), shown in Fig. S5 and Table S2 of the supplementary file, the composite with 30 mass% of lyocell has an onset temperature of degradation and temperature (T_{onset}) of maximum degradation rate (T_{max}) of 331 °C and 346 °C, respectively, while neat PLA has a T_{onset} and T_{max} of 344 °C and 368 °C, respectively.

All the filaments could be successfully printed into the samples with good precision and surface quality. Even the formulations with 30 mass % of fibres did not present any issues during printing. This can be observed in Fig. 3b, where a disk printed using the L30-MA filament and the printing parameters given in Table 2 has the same dimensions as the drawing used to generate the G-code. Additional testing was conducted to assess the dimensional accuracy using neat PLA and composite filaments with 10–30 mass% of lyocell fibres. Samples of the same size as the ones used for DMA testing (Fig. 2b) were 3D printed using the parameters of Table 2 and measured. The difference between the 3D-printed composite samples and the.stl drawing was in the order of 1% for the length, and maximum of 3.4% for width and −2% for thickness (Table S1). This difference in the dimensions is similar to the obtained values for neat PLA and PLA-MA. In fact, the printability of the lyocell-reinforced composites is similar to PLA and there is no need to modify the 3D printing parameters. Even the thermal conductivity of PLA and the composite with high fibre content is similar (results summarised in Table S2). It is worth noting that a large nozzle (0.75 mm) was used in this study to avoid clogging issues, which has a direct effect on the dimensional accuracy of the 3D-printed objects. It is expected that smaller nozzles would improve the 3D printing finishing, but further study is needed.

In this study, the combination of three strategies to improve the fibre/matrix interface and, thereby, the mechanical properties of the composites were used; (i) modification of PLA using MA as a coupling agent, (ii) fibre fibrillation, and (iii) post-printing heat treatment. First, the effects of using MA and heat treatment are discussed, followed by the influence of fibre fibrillation on the mechanical performance of the composites.

The tensile properties of the 3D-printed samples are given in Table 3, organised according to the use of MA (samples with -MA) and the post-printing heat treatment. The tensile strength (TS), Young's modulus (E), strain at break (ε_b), and limit of proportionality (LOP) were calculated for each condition. The LOP was determined according to ASTM D638. It was calculated as the stress where there is a decrease in the correlation factor of the linear region of the stress/strain curve, leading to a drop of 4% in Young's modulus. The first thing to observe is that the addition of lyocell fibres without any modification led to a small decrease in the TS of PLA. Interestingly, the formulations with 10–30 mass% of fibres

Table 3
Average (Avg.) tensile properties of 3D printed lyocell/PLA composites in the as-printed and heat-treated conditions.

Condition	Tensile strength in MPa		Limit of Proportionality in MPa*		Young's Modulus in GPa		Strain at break in %	
	Avg.	COV	Avg.	COV	Avg.	COV	Avg.	COV
As-printed								
PLA	65.3^{d}	0.02	32.6^{d}	0.07	3.46^{g}	0.07	6.67^{a}	0.04
L10	58.8^{e}	0.01	33.3^{d}	0.02	4.16^{f}	0.02	6.19^{a}	0.03
L20	58.6^{e}	0.01	34.3^{d}	0.01	$4.63^{d,e}$	0.01	3.93^{b}	0.02
L30	58.4^{e}	0.06	$35.9^{c,d}$	0.06	5.05^{c}	0.06	$2.86^{b,c}$	0.05
PLA-MA	57.2^{e}	0.02	$35.1^{c,d}$	0.09	3.32^{g}	0.09	3.96^{b}	0.07
L10-MA	60.8^{e}	0.02	33.9^{d}	0.05	$4.37^{e,f}$	0.05	5.74^{a}	0.02
L20-MA	$66.8^{c,d}$	0.02	$38.6^{b,c}$	0.04	5.23^{c}	0.04	3.71^{b}	0.04
L30-MA	70.5^{c}	0.01	41.8^{b}	0.02	5.93^{b}	0.02	3.38^{b}	0.02
Heat-treated								
L10-HT	65.6^{d}	0.03	41.6^{b}	0.03	$4.95^{c,d}$	0.03	3.67^{b}	0.05
L20-HT	64.8^{d}	0.01	39.6^{b}	0.02	5.34^{c}	0.02	3.55^{b}	0.02
L30-HT	60.2^{e}	0.05	41.4^{b}	0.03	5.97^{b}	0.03	1.62^{c}	0.04
L10-MA-HT	$66.9^{c,d}$	0.02	39.7^{b}	0.03	$5.00^{e,f}$	0.03	3.73^{b}	0.02
L20-MA-HT	74.8^{b}	0.02	46.2^{a}	0.05	6.03^{b}	0.05	3.52^{b}	0.03
L30-MA-HT	78.8^{a}	0.02	48.1^{a}	0.02	6.75^{a}	0.02	3.15^{b}	0.04

Values in the same column with different superscripts (a-g) are significantly different ($p \leq 0.05$). *Limit of Proportionality (LOP) = considered as the stress where there is a 4% decrease in Young's modulus (as per ASTM D638).

presented similar values of TS (58 MPa) but the LOP was slightly improved when the fibres were added (although not statistically relevant). The Young's modulus of the composites was improved in comparison with neat PLA, achieving a maximum value of 5.05 GPa.

These results indicate that the load transfer between fibre and matrix is insufficient to provide efficient reinforcement. Considering that the fibres used in this study are very short (more about that in the next sections), there is a high probability that the fibres have a length lower than (or close to) the critical fibre length, which is around 0.30 mm for the diameter of these fibres [10]. Due to the small fibre diameter and the limited breaking force of the fibre, it has not yet been possible to determine the adhesion between lyocell 1.3 dtex and a PLA matrix as it is very difficult to apply PLA droplets small enough for this fibre. As a result, the breaking force of the fibre was exceeded in many cases during the microbond test and the fibres broke before a fibre pull-out occurred. However, the critical fibre length of lyocell with a fineness of 1.3 dtex (as used in this study) in combination with a PLA matrix could be theoretically calculated in a former study based on the results of lyocell fibres with a fineness of 15.0 dtex. The critical fibre lengths for lyocell of 1.3 dtex in PLA (without any modification of the fibre or matrix) ranged between 0.22 mm and 0.30 mm [68].

The addition of MA in the modified formulations had a negative effect on the tensile properties of the matrix. The PLA-MA formulation had a slight decrease in the TS and strain at break. This effect is attributed to possible chain scission of the polymer with the addition of DCP and MA during compounding, reducing the molecular mass of PLA [40,69]. Even additions as low as 2 mass% of MA have been demonstrated to drastically decrease PLA's weight-average molecular mass [70]. This effect was observed by the drop in the torque values when MA and DCP were added during the compounding process. Nonetheless, this modification had a positive effect on the tensile properties of the composites with the increase in fibre content. In this case, it is possible to observe a statistically significant and gradual increase in TS and E with the addition of lyocell fibres, achieving a TS up to 70.5 MPa and E up to 5.93 GPa, which is 23% and 78% higher, respectively, than those for neat PLA-MA. A significant increase in the LOP was also observed (from 35.1 MPa to 41.8 MPa). The increase in TS, E, and LOP indicates a good interfacial bonding between the fibres and the matrix, in a situation where load is being effectively transferred to the fibres. This effect can be visualised in Fig. 4, where the fracture surfaces of the samples with 30 mass% of fibres are shown. The 3D printed samples have a well consolidated morphology with almost no presence of inter-bead porosity, which demonstrates that the printing parameters (Table 2) were adequate. In the fracture surface of the composites, it is possible to observe a lower content of voids created by the pull-out of fibres in the sample modified with MA (white arrows), indicating better fibre/matrix interfacial bonding. In addition, the composites presented strain at break values higher than composites reinforced with natural fibres, which shows the

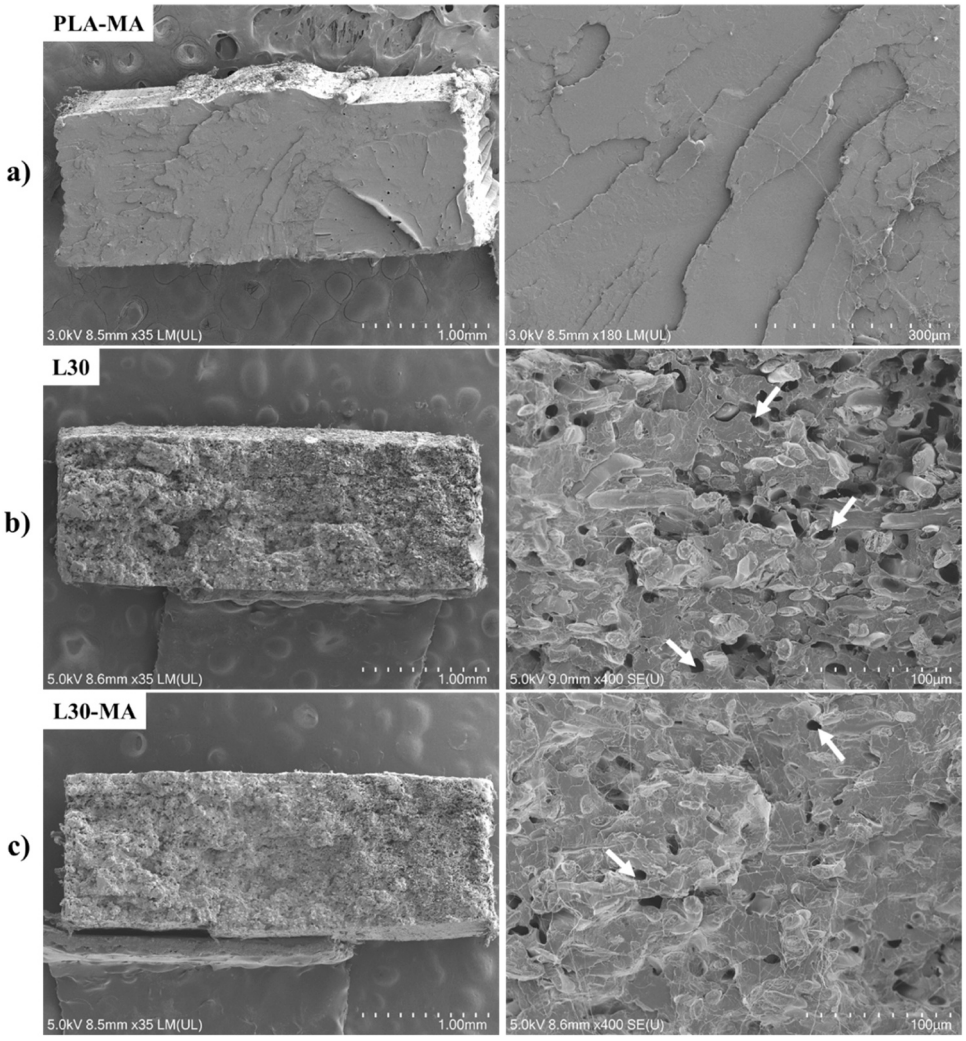

Fig. 4. SEM micrographs of fracture surfaces of 3D printed PLA-MA (a) and composites with 30 mass% of lyocell fibre (b-c). The white arrows in Figures b) and c) indicate the voids created by the pull-out of fibres.

advantages of using lyocell fibres. Composites with high content of short natural fibres, such as hemp, bamboo, and wood fibres, have low strain at break, generally below 2%. This is expected considering the mechanical properties of the single fibres. Lyocell fibres have a strain at break of 11–16% [28], while most natural lignocellulose fibres have a strain at break between 1% and 5% [1].

The main objective of modifying PLA with MA was to improve the interfacial bonding between PLA and the lyocell fibres. It is hypothesised that two mechanisms were involved in improving the mechanical performance of the composites. First, with the decrease in the molecular mass of PLA with the addition of MA and DCP, there was also a decrease in the viscosity of the polymer during compounding, which contributed to better wetting of the fibres and, consequently, a higher surface area between fibre and matrix was available to transfer the load applied during tensile testing. Second, the MA grafted into PLA works as a coupling agent, improving the chemical compatibility between the fibres and the matrix and thereby increasing the interfacial shear strength of the lyocell fibres in PLA. However, reactive extrusions used to add coupling agents, such as MA, into PLA structure lead to a poor degree of grafting and loss of molecular mass because of the oxidative susceptibility of PLA [70]. We were not able to observe evidence of grafted MA into PLA's structure by using nuclear magnetic resonance (NMR) analysis of polymer samples extracted from the modified composites and purified in methanol (results presented in the Supplementary Information). This indicates that the methodology used in this study resulted in a very low grafting degree. Nonetheless, promising mechanical properties were obtained by modifying the matrix with MA, which may be attributed to the first mechanism (although a very low degree of grafting may have also contributed to the improved mechanical performance). The improvement in the fibre/matrix adhesion with the modification using MA is further elucidated in Section 2.5.6. (DMA analysis).

The mechanical properties of the composites after post-printing annealing were also assessed. Table 3 gives the resulting TS, LOP, E, and ε_b of the PLA and PLA-MA-based composites. The neat PLA and PLA-MA samples could not be tested because they shrank and warped after heat treatment (Fig. 5a-b). The same effect is reported in [10]. This PLA grade has a low heat deflection temperature and shrinks when the crystallinity increases. We observed that this effect is absent if fibres are added to the composites. All the formulations reinforced with lyocell fibres had a significant increase in the TS, LOP, and E after annealing, in special formulations modified with MA. The L30-MA sample achieved a TS of 78.8 MPa and E of 6.75 GPa, which is 11.8% and 13.8% higher, respectively, than the as-printed samples. This was an improvement of 37.8% for TS and 103% for E in relation to neat PLA-MA. It is worth mentioning that the slight decrease in strain at break of the composites was not statistically relevant after annealing. In Fig. 5(c), it is possible to observe that even the formulation with high fibre content presented a well-defined "plastic" deformation region before failure, which shows the improved toughness of the composites with the addition of fibres. This behaviour has not been reported in any publication related to 3D printed composites reinforced with high content of natural fibres.

Fig. 6 shows SEM micrographs of the fracture surface of L30-MA 3D printed samples in the as-printed and heat-treated conditions. It is possible to observe that after heat treatment, there is a lower content of gaps between the matrix and the fibres, which may have contributed to better interfacial bonding between fibre and matrix and, therefore, have led to improved mechanical properties. Furthermore, it is possible to observe thin polymer strands attached to the fibres (white arrows), which is believed to be an indication of strong interfacial bonding between fibre and matrix [4].

The improvement in the tensile strength of the heat-treated composites can also be explained by the increase in the PLA crystallinity, which has been demonstrated to have positive effects on the mechanical properties of PLA [71,72]. The DSC results of the as-printed and heat-treated samples are given in Table 4, and selected DSC curves are shown in Fig. 7. From this Figure, three transitions representing the glass transition temperature (T_g), cold crystallisation temperature (T_{cc}), and melting temperature (T_m) can be identified. Since we wanted to evaluate the thermo-physical properties of the printed samples, only the results of the first heating cycle are reported. The crystallinity of PLA (X_c) of all the samples calculated using Eq. (1) is given in Table 4. It is possible to observe a considerable increase in X_c after heat treatment in all the analysed samples, from 3.5% to 7.6% to 29–34%. It is hypothesised that the printing orientation also influences the improvement observed in this study. During printing, the PLA molecular chain is aligned with the printing direction [73]. When the PLA is heat treated, the crystalline PLA is also oriented in the printing direction (and therefore in the loading direction), which may contribute to higher TS and E.

As can be observed in Table 4, there was a decrease in the T_{cc} with the addition of fibres, indicating that the fibres influence the crystallisation behaviour of PLA. As the fibres can be nucleation sites for the heterogeneous formation of PLA crystals; generally, a reduction in the T_{cc} or faster crystallisation kinetics is reported with the addition of fibres [4,44,74]. Although the addition of fibres seems not to influence the T_g, the addition of MA decreased the T_g of PLA slightly, which may be an indication of the reduced molecular mass of PLA. In addition, metastable and imperfect crystals (α') may form during 3D printing and also due to the crystallisation effects of the fibre on PLA [4,75]. This effect results in a bimodal melting endotherm, as the ones in the heat-treated samples with high content of fibre shown in Fig. 7. In this case, the first peak of

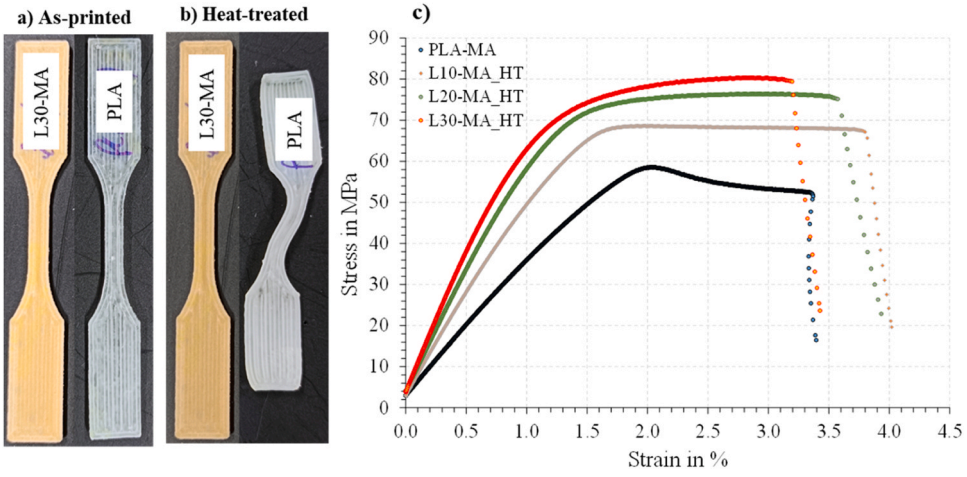

Fig. 5. Tensile test samples before (a) and after (b) heat treatment. Stress/strain curve of 3D printed samples of neat PLA and heat-treated composites with 10–30 mass% of fibre content (c).

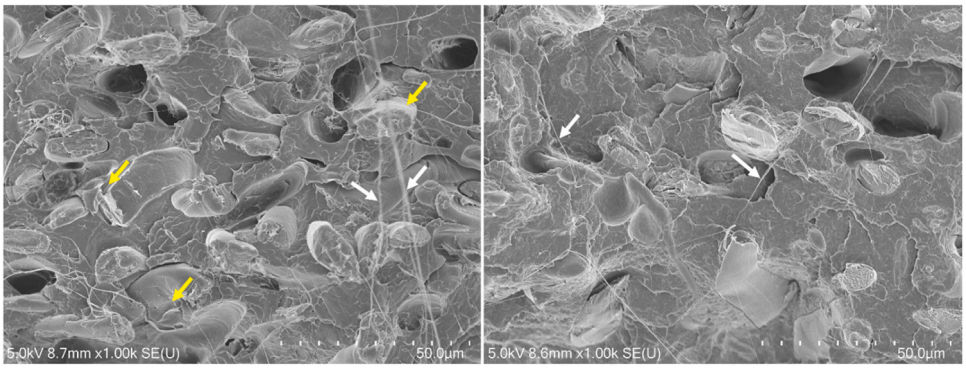

Fig. 6. SEM micrographs of the fracture surfaces of L30-MA samples in the as-printed (left) and heat-treated conditions (right). The yellow arrows indicate the gap between the matrix and fibres and the white arrows indicate the polymer strands.

Table 4
Summary of DSC results of as-printed and heat-treated 3D printed samples.

Sample	T_g in °C	T_c peak in °C	ΔH_c in J/ g_{PLA}	T_m peak in °C	ΔH_m in J/ g_{PLA}	X_c in %
As-printed						
PLA	60.2	114.3	-26.69	152.4	27.18	0.53
PLA-MA	58.3	119.7	-21.37	151.3	22.08	1.04
L10	61.5	112.5	-23.83	151.6	27.06	3.46
L10-MA	61.0	113.0	-26.58	151.5	29.20	2.82
L20	60.9	113.2	-23.69	150.2	29.33	6.06
L20-MA	60.7	112.7	-24.30	151.5	31.40	7.63
L30	59.3	109.8	-24.69	151.1	30.76	6.53
L30-MA	60.6	111.0	-21.84	151.7	28.01	6.64
Heat-treated						
PLA-HT	-	-	-	151.7	24.97	26.8
PLA-MA-HT	-	-	-	150.6	24.7	26.6
L10-HT	-	-	-	152.3	28.53	30.7
L10-MA-HT	-	-	-	150.9	27.83	29.9
L20-HT	-	-	-	151.0	27.20	29.2
L20-MA-HT	-	-	-	150.1	28.78	30.9
L30-HT	-	-	-	151.1	31.47	33.8
L30-MA	-	-	-	151.0	26.83	28.8

T_c –Crystallisation temperature; T_g – Glass transition temperature; Tm – Melting temperature; H_c –Crystallisation heat; ΔH_m – Heat of melting; X_c – PLA crystallinity.

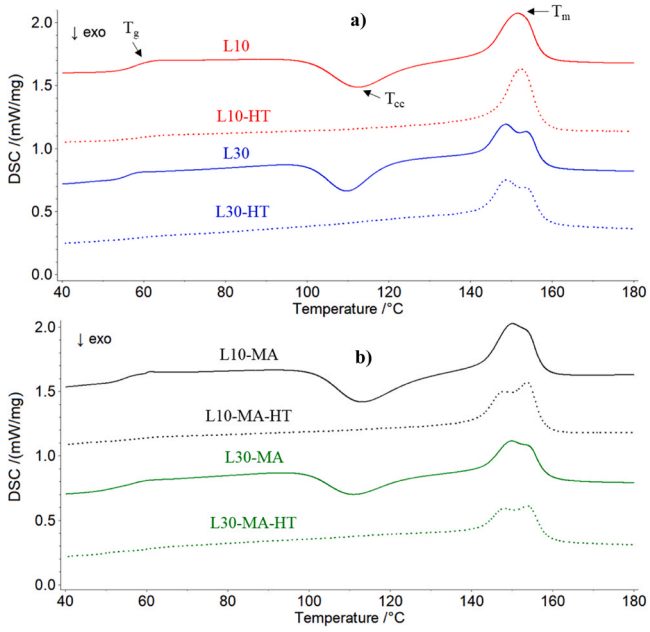

Fig. 7. DSC curves of PLA (a) and PLA-MA (b) composites in the as-printed and heat-treated conditions.

fusion is related to the simultaneous melting of primary α crystals and recrystallisation of α' to α, while the second peak of fusion is the heat related to the melting of the α crystal formed in the recrystallisation process.

3.1.1. *Effect of fibre fibrillation*

Fibre fibrillation was also used in this study as a strategy to improve the mechanical performance of the composites. SEM images of the as-received and fibrillated fibres in the longitudinal direction are shown in Fig. 8. First, it is possible to observe that the as-received fibres have a very smooth surface, which is not positive for a strong mechanical interface between matrix and fibre. However, with the fibrillation process, it was possible to create nanofibrils (yellow arrows) and grooves (white arrows) on the surface of the lyocell fibres. It is also noteworthy that this modification takes place mainly on the outer surface of the fibres, and therefore, it is not expected to cause significant changes in the mechanical properties of the fibres. The nanofibrils shown in Fig. 8 have a width of approximately 100–300 nm, which is slightly smaller than the size range reported by Tanpichai et al. (between 350 and 500 nm) [76], and within the range reported by Graupner et al. (between 100 and 400 nm) [48]. Interestingly, although we used the same fibrillation procedure in this work and our previous work [48], the fibrillation was more pronounced in the former one. One possible explanation is that the fibres in the first study were much coarser (15 dtex) than those used in this work (1.3 dtex). The increased content of defects in coarser fibres produced by the lyocell process may facilitate the debonding of nanofibrils from the surface, resulting in a higher degree of fibrillation. It is also possible that fibrils have completely separated from the bulk fibre due to the short fibre length. In the previous study, long fibres (~60 mm) were used for fibrillation and it could be seen that some of the fibrils split off from the bulk fibre over lengths of 1–2 mm. Since the fibres used here had average fibre lengths < 300 µm, it is possible that fibrils have completely separated from the bulk fibre over the length and were present separately in the solution and partly in the matrix. When the fibrillation process was carried out, it was observed that there was a considerable amount of fine particles (probably nano fibrils) in the solution that had settled after fibrillation, which strengthens the aforementioned hypothesis.

It is expected that the increase in surface roughness and increased surface area with the presence of nanofibrils will contribute to a better anchoring of the lyocell fibre in the PLA matrix, resulting in a similar effect reported in [48]. Therefore, the effect of lyocell fibre fibrillation was assessed in the composites with high fibre content (30 mass%), with and without the addition of MA. The effect of post-printing annealing

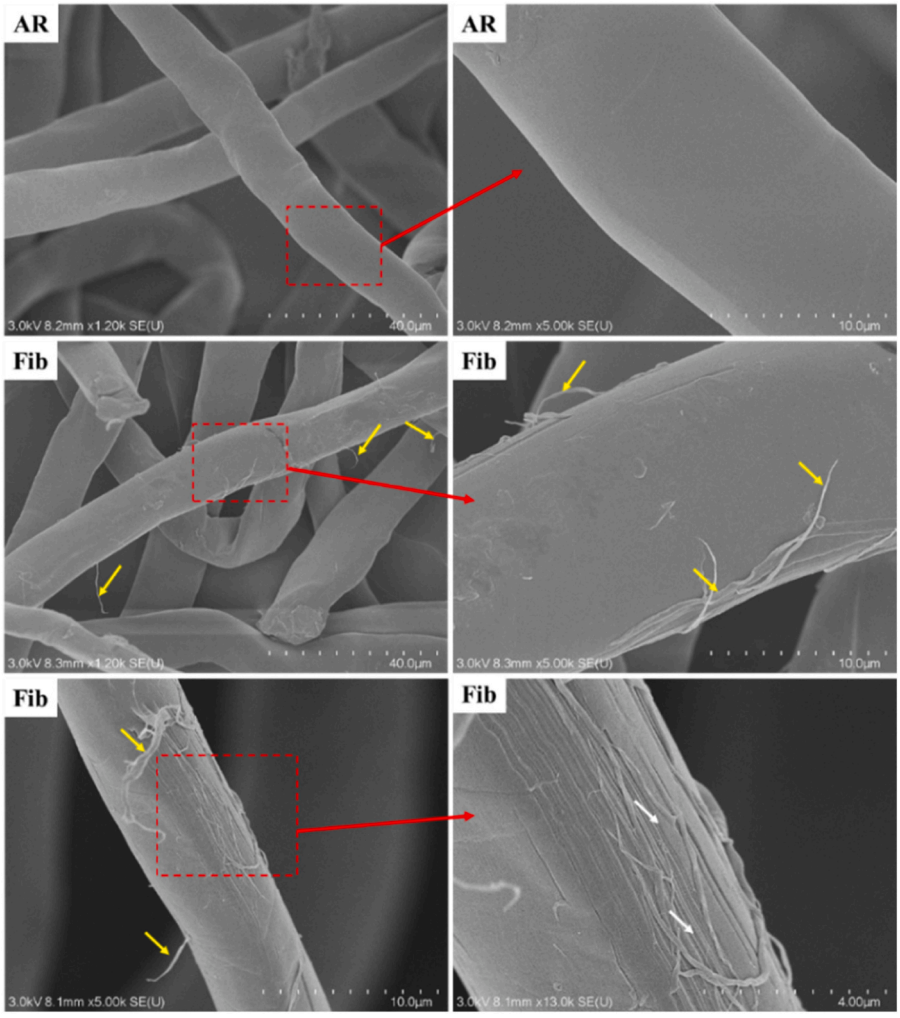

Fig. 8. SEM image of as-received and lyocell fibre after the fibrillation process, where AR=As-received fibres and Fib=Fibrillated fibres. The yellow and white arrows indicate the fibrils and "grooves" formed by the fibrillation process.

was also evaluated in the 3D-printed samples reinforced with the fibrillated fibres. The obtained tensile test results and crystallinity of PLA (X_c) of the composites with 30 mass% of fibres are given in Table 5.

From the results shown in Table 5, it can be observed that by using fibrillated lyocell fibres, better TS, LOP and E were obtained even without the addition of MA. The L30fib formulation had an improvement of 18.4% for TS and 14.0% for E compared with the composite with unmodified fibres and had similar tensile properties as the formulation modified with MA. By combining the fibrillated fibres and the PLA modified with MA, we obtained the best tensile properties for these composites, achieving a TS, LOP, and E of 76.6 MPa, 43.7 MPa, and 6.44 GPa, respectively, while maintaining a strain at break of 3.67%. These results represent an improvement of 31.2% in TS and 27.5% in E compared to the composite with untreated fibres and unmodified matrix (L30).

In order to assess if the improvement in the mechanical properties of the composites with fibrillated lyocell was related to the fibre length, we also analysed the length of the fibres before processing, e.g., the as-

Table 5
Average (Avg.) tensile properties of 3D printed lyocell/PLA composites produced using fibrillated fibres in the as-printed and heat-treated conditions.

Condition	Tensile strength in MPa		Limit of Proportionality in MPa*		Young's Modulus in GPa		Strain at break in %		X_c in %* *
	Avg.	COV	Avg.	COV	Avg.	COV	Avg.	COV	
As-printed									
L30	58.4^{d}	0.06	35.9^{e}	0.06	5.05^{f}	0.06	2.86^{c}	0.05	6.53
L30fib	69.2^{c}	0.03	40.2^{d}	0.05	5.76^{e}	0.05	$3.37^{a,b}$	0.03	5.13
L30-MA	70.5^{c}	0.01	41.8^{d}	0.02	$5.93^{d,e}$	0.02	$3.38^{a,b}$	0.02	6.64
L30fib-MA	76.6	0.04	43.7^{c}	0.03	$6.44^{b,c}$	0.03	3.67^{a}	0.08	6.02
Heat-treated									
L30-HT	60.2^{d}	0.05	41.4^{d}	0.03	$5.97^{d,e}$	0.03	1.62^{d}	0.04	33.8
L30fib-HT	76.9^{b}	0.02	48.3^{b}	0.03	$6.31^{c,d}$	0.03	2.76^{c}	0.02	32.7
L30-MA-HT	78.8^{b}	0.02	48.1^{b}	0.02	6.75^{b}	0.02	$3.15^{b,c}$	0.04	28.8
L30fib-MA-HT	85.0^{a}	0.03	51.0^{a}	0.03	7.18^{a}	0.02	$3.19^{b,c}$	0.12	30.9

Values in the same column with different superscripts (a-g) are significantly different ($p \leq 0.05$). *Limit of Proportionality (LOP) = considered as the stress where there is a 4% decrease in Young's modulus (as per ASTM D638). **PLA crystallinity (X_c) calculated using Eq. (1) using DSC measurements.

received (UT) and fibrillated fibres (Fib) and the fibres extracted from the 3D-printed composites with 30 mass% of fibres. The boxplot graph of all the analysed conditions is shown in Fig. 9, and the corresponding average and standard deviation are given in Table 6. Before compounding, the fibrillated fibres (286 μm) are slightly longer than the untreated fibres (203 μm). During the fibrillation process of the fibres, different cycles of wetting and draining/filtering were conducted, which may have removed some of the fines present in the as-received fibres. In both cases, the average fibre length is considerably lower than the nominal length of the lyocell fibres (400 μm) indicated by the manufacturer. After compounding, filament production, and 3D printing, there was a significant overall decrease in fibre length. All 4 formulations presented similar fibre lengths, between 116 and 134 μm, which represents a reduction of approximately 55% for the formulations with fibrillated fibres and 42% for the formulations with unmodified fibre. Therefore, it is reasonable to assume that fibre length did not have a significant role in the difference in the tensile properties given in Table 5, with the improvement in the interfacial bonding (attributed to the presence of nanofibrils) the main factor.

Similar to what was reported previously, by increasing PLA's crystallinity, it was possible to improve even more the mechanical properties of the composites with a high content of lyocell fibres. The resulting tensile properties and PLA's crystallinity of the unmodified and modified 3D printed composites after annealing are also shown in Table 5. It is evident that the heat treatment was beneficial for all the formulations, and by using the combination of fibre and matrix modification and post-printing treatment, we were able to achieve very promising mechanical properties, e.g., tensile strength of 85 MPa, Young's modulus of 7.18 GPa, and strain at break of 3.19%. These values represent an improvement of 30% in TS and 107% in Young's modulus in relation to 3D-printed neat PLA (49% and 116%, respectively, in relation to PLA-MA) without significantly sacrificing strain at break. In addition, an increased PLA crystallinity is expected to improve the thermo-mechanical behaviour of the composites, which would help overcome one of the biggest problems of PLA, which is its mechanical instability at moderate temperatures (around 50–60 °C).

Fig. 10 shows the stress-strain curves and SEM images of the fracture surfaces of the worst (L30) and best (L30fib-MA-HT) formulations presented in Table 5. It is clearly noticeable that the L30 formulation has a high void content caused by the pull-out of fibres (yellow arrows). This effect was reflected by the poor TS and limited E observed for this formulation. In the L30fib-MA-HT sample, on the other hand, there are much fewer voids caused by fibre pull-out, and it is possible to observe the cross-section of fractured fibres, indicating that they achieved their maximum stress with the fracture of the composite. In addition, the fibres are uniformly distributed and completely wetted/surrounded by the polymer. Some voids possibly related to defects during printing (white arrows) can also be observed in the samples shown in Fig. 10.

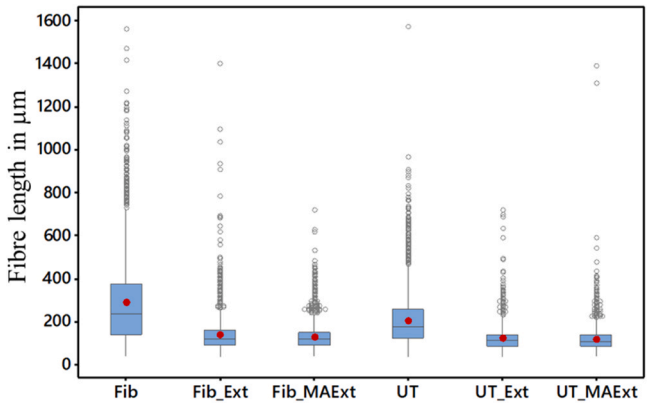

Fig. 9. Boxplot of fibre length of lyocell fibres before processing and after extraction from the composite filaments with 30 mass% of lyocell fibres. The red dots represent the arithmetic average of the measurements, and the grey circles are the outlier values. Fib=fibrillated fibres and UT=Untreated fibres. The condition names with the "Ext" suffix are the fibres extracted from the composites with 30 mass-% of fibres.

Table 6
Summary of average fibre length of lyocell fibres before and after processing into composites. Fib=fibrillated fibres and UT=untreated fibres. The condition names with the "Ext" suffix are the fibres extracted from the composites with 30 mass% of fibres.

Sample	Condition	N	Average length in μm	Standard deviation
Fib	Before processing	3223	285.6	192.3
Fib_Ext	Extracted from 3D	6327	133.9	68.4
Fib-MAExt	printed sample	26,609	124.6	49.8
UT	Before processing	8494	203.3	111.8
UT_Ext	Extracted from 3D	12,692	117.5	46.9
UT_MAExt	printed sample	19,207	116.4	46.7

From Fig. 10, it is possible to observe that mainly the cross-section of the fibres is visible in the fracture surfaces, which indicates that the fibres have a preferential orientation. During the production of the filament and 3D printing, the shear forces present in the exit nozzle can induce fibre alignment. This effect can be influenced by the nozzle size and extrusion/printing speed [77]. In our case, the shear rate during printing ($\dot{\gamma}$) for a 0.75 mm nozzle and printing speed of 1800 mm/min is estimated to be $\dot{\gamma}$= 54.3 s^{-1}.

In order to verify further the alignment of the lyocell fibres, we also conducted an XRD analysis of a 3D-printed sample in transmission mode. The orientation of the fibres can be observed by the change in the diffracted intensity of cellulose planes across the azimuthal (ϕ) axis. In this case, a fixed 2θ angle of approximately 21° was used for the azimuthal scan. Lyocell fibres have a cellulose II crystalline structure, and this 2θ angle is related to the diffraction of the (110) and (020) planes of cellulose II structure (Fig. 11a) [10,78]. The 2θ scans using azimuthal angles at 0° and 90° shown in Fig. 11b, indicate a considerable difference in the diffracted intensity in the 2θ range corresponding to the cellulose planes (110) and (020), between 19° and 24°. This effect is better visualised in Fig. 11c, which shows the corresponding azimuthal scan of the 3D-printed sample and the control sample with randomly-oriented untreated lyocell fibres. The degree of ordering (π) and Herman's order parameter (f) can be used to determine the degree of cellulose alignment in each condition. The degree of ordering (π) and Herman's order parameter (f) can be calculated using Eqs. (2) and (3) [79]:

$$\pi = \frac{180 - FWHM}{180} \tag{2}$$

where FWHM is the full-width half maximum of the analysed peak in an azimuthal scan.

$$f = \frac{3 < \cos^2 l > -1}{2} \tag{3}$$

where:

$$< \cos^2 l >= 1 - 2 < \cos^2 \theta > \tag{4}$$

and

$$< \cos^2 \theta >= \frac{\int I(\varphi)\cos^2\varphi \sin\varphi d\varphi}{\int I(\varphi)\sin\varphi d\varphi} \tag{5}$$

where θ and φ are the angles related to 2θ and azimuthal positions, respectively. A Herman's parameter of f= 1 corresponds to a maximum orientation, whereas f= 0 indicates random orientation. For the degree of ordering, the closer to 100% the obtained value is, the more aligned the crystal lattices of cellulose are to a specific direction.

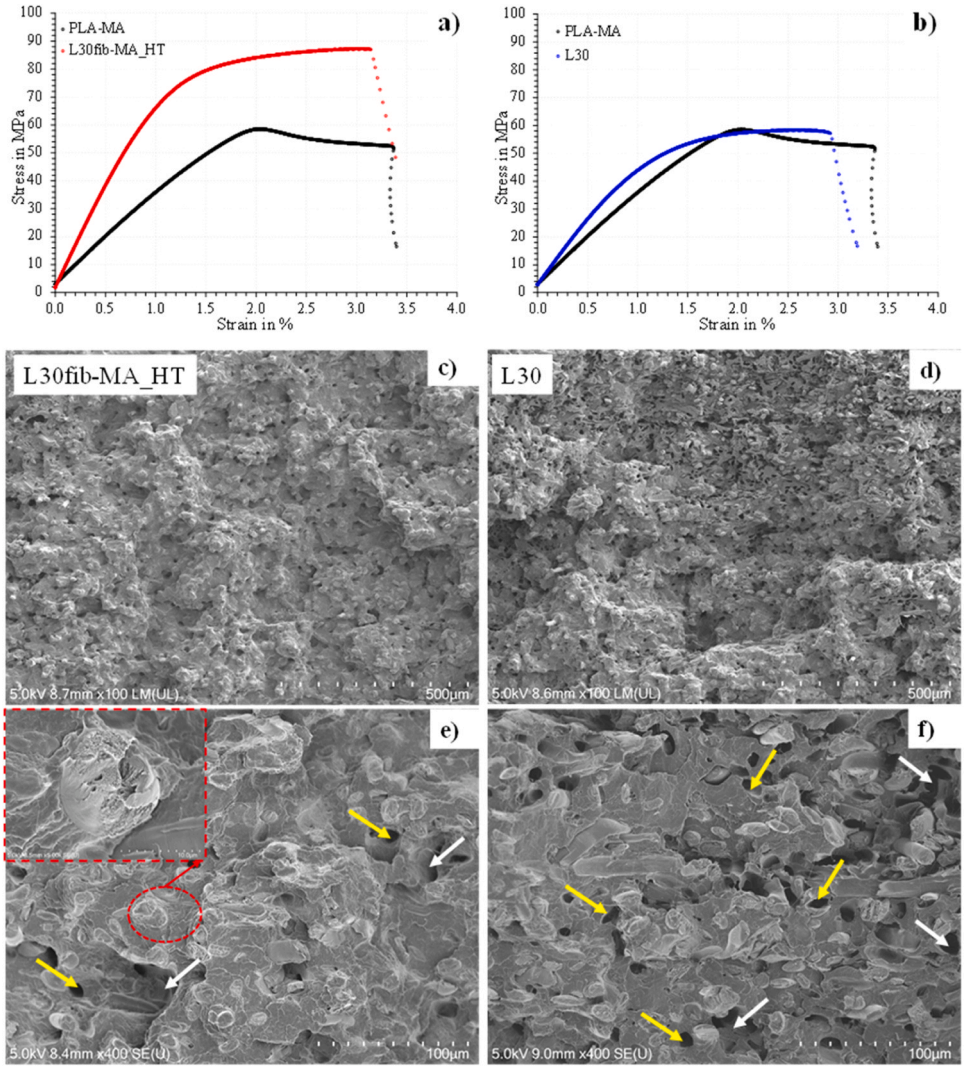

Fig. 10. Stress-strain curves of the 3D printed L30fib-MA_HT (a) and L30 (b) samples in comparison with PLA-MA and corresponding SEM images of the fractured surfaces of the L30fib-MA_HT (c,e) and L30 (d,f) samples. The yellow arrows show holes caused by the pull-out of fibres, and the white arrows show possible voids in the 3D-printed samples.

The degree of ordering (π) and Herman's parameter for the 3D printed samples with 30 mass% of fibrillated fibres are 74.7% and 0.620, respectively. These values indicate that the lyocell fibres in the 3D-printed composite have a preferred orientation. This effect can be visualised in Fig. 11c, where the diffraction scan along the azimuthal axis of the 3D printed sample has a peak at around 90°. In comparison, the compressed "mat" made of as-received lyocell fibres with random orientation has the same intensity throughout the entire scan. This result corroborates with the SEM images of the fractured 3D printed samples, which revealed that most of the observed fibres were perpendicular to the plane of fracture.

By using a combination of fibre fibrillation, matrix modification and post-printing annealing, we were able to obtain a considerable improvement in the mechanical properties of PLA. Although the fibres in all the composite formulations are noticeably short (approximately 125 µm), it was possible to effectively align the fibres in the loading direction using 3D printing. Therefore, the improved mechanical properties of our composites are attributed not only to an enhanced interfacial bonding between fibre and matrix but also because the fibres are aligned in the printing direction. In Fig. 12, our results are compared with the tensile strength and Young's modulus reported in the literature for 3D printed composites reinforced with short fibres. Short natural fibres and synthetic fibres, such as carbon and glass fibres, are shown, including research-only and commercial composites. We obtained the highest value for tensile strength reported to date from the selected references for this class of composites. In addition, a good balance between tensile strength, Young's modulus and strain at break was achieved in this study. Two works obtained the same or higher Young's moduli than our composites [9,16], but the strain at break of these composites is relatively lower than ours. In these two studies, the samples were also printed using a raster angle of 0° (parallel to the loading direction during tensile testing) and the composites had 30 mass% of fibres but they used different fibres; nanofibrillated cellulose [16] and harakeke (NZ flax) [9].

The printing raster angle plays a crucial role in the final mechanical properties of a printed object. One of the advantages of being able to control the alignment of the reinforcing fibres selectively is that parts of the object subjected to higher stresses can be printed with the fibres aligned to the loading direction. However, obtaining isotropic mechanical properties is also desired in some applications. Therefore, we also evaluated the effect of the printing raster angle on the tensile properties of neat PLA and heat-treated L30fib-MA composite, which is the condition with the best tensile properties. The results for TS and Young's modulus are summarised in Fig. 13. Neat PLA is not considerably affected by the printing orientation; however, the best tensile strength is obtained when the printing direction is parallel to the loading

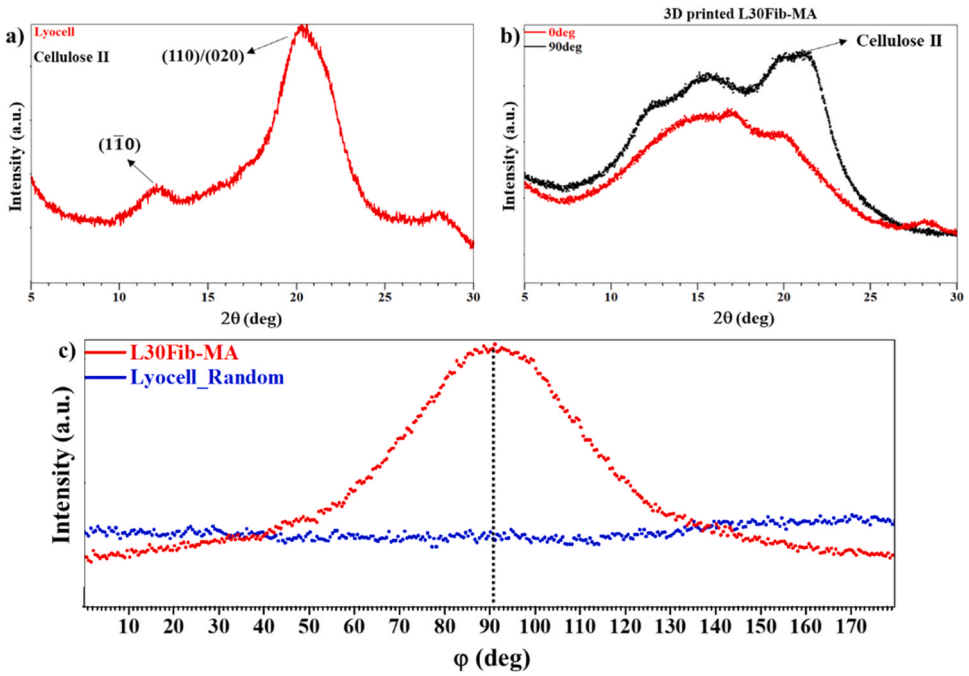

Fig. 11. XRD 2θ scans of neat lyocell fibres (a) and 3D printed L30Fib-MA composite measured at ϕ angles of 0° (red line) and 90° (black line) (b). Azimuthal (ϕ) scans between 0° and 180° of random lyocell fibres mat (blue line) and 3D printed L30Fib-MA composite (red line) (c).

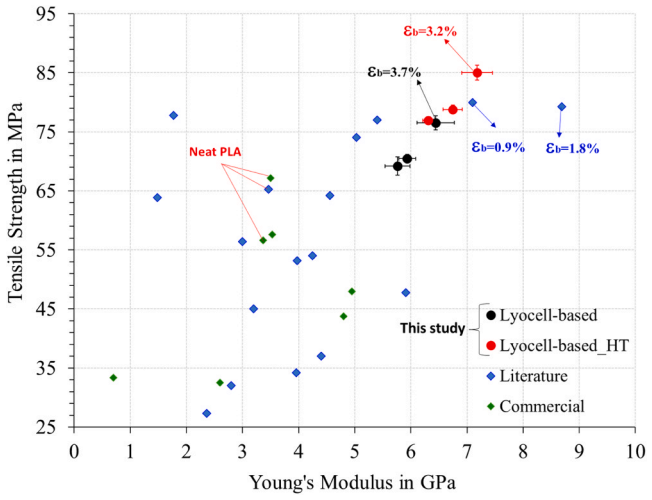

Fig. 12. Tensile properties of PLA/lyocell composites developed in this work compared to other 3D printed PLA-based composites. Results of tensile tests of samples printed using 100% infill with raster angles of +45/−45° or 0°. Only the best results obtained in each reference are shown. Literature – PLA composites using the following fibres: hemp, microcrystalline cellulose, nanofibrillated cellulose, flax, wood, basalt fibre, bamboo, lyocell, harakeke, curaua, carbon fibre, heneken [9,10,16,52–55,80,81–87]. Commercial – neat PLA or composites using the following fibres: bamboo, short carbon fibre, and wood [88–95]. ε_b = Strain at break. The error bars indicate one standard deviation.

direction, which is commonly reported [73]. Considering the alignment of fibres during printing, anisotropy is expected in the case of L30fib-MA composite. Indeed, the composite has the highest tensile properties when the loading direction is parallel to the printing direction. At a 90° angle, the tensile strength is comparable to PLA, but the composite has a higher Young's modulus. If the sample is produced with alternating layers printed at 0° and 90°, the TS is also comparable to PLA, but a much higher Young's modulus is obtained, an increase of 65% in comparison with neat PLA. Only a few works addressed the effect of printing orientation on the mechanical properties of fibre-reinforced PLA, but in most cases, a considerable drop in tensile strength is seen in composites printed with a raster angle of 90°, generally lower than neat PLA.

3.1.2. Thermo-mechanical stability

Dynamic mechanical analysis (DMA) is generally used to assess the thermo-mechanical stability of polymers and composites by obtaining their viscoelastic properties at different temperatures, which can be represented by the storage modulus, loss modulus, and damping factor (known as tanδ) [96]. The storage modulus (E') and tanδ curves for the different formulations with 30 mass% of fibre, neat PLA, and PLA-MA are illustrated in Fig. 14. The curves for the heat-treated composites are also shown in the same Figure. A summary of properties obtained from the curves shown in Fig. 14 is given in Table 8.

The E' is related to the elastic energy stored by the material during the loading and unloading cycles, and it is usually improved by the addition of reinforcing fibres [4,9,16]. The damping factor, tanδ, is the ratio between loss modulus and storage modulus and the temperature of its maximum value indicates the glassy-to-rubbery transition, which can be considered as the glass transition temperature (T_g). Lower values of the tanδ peak also indicate a less pronounced glassy-to-rubbery transition and a predominance of elastic behaviour. Fig. 14a shows a steep drop in the E' at around 60 °C for all the formulations, which is related to the glassy-to-rubbery transition. However, there is an evident increase in the E' for the composites in comparison with neat PLA. At higher temperatures, the absolute E' values are quite low, but the difference between the composites and neat PLA is more pronounced (up to 60x higher than neat PLA). This means that the fibres are preventing the mobility of PLA molecules in the rubbery region, which is also confirmed by the considerable decrease in the tanδ peaks (Fig. 14c). The modification with MA was detrimental to the thermo-mechanical stability of PLA, which is evidenced by a decrease in the T_g temperature and lower E' values at higher temperatures. Although less pronounced, the composites with MA were also affected. As previously mentioned, this effect is attributed to the decrease in the molecular mass of PLA during the compounding with MA.

Besides the influence of the fibres improving the thermo-mechanical stability of PLA, the presence of crystalline regions also decreases the

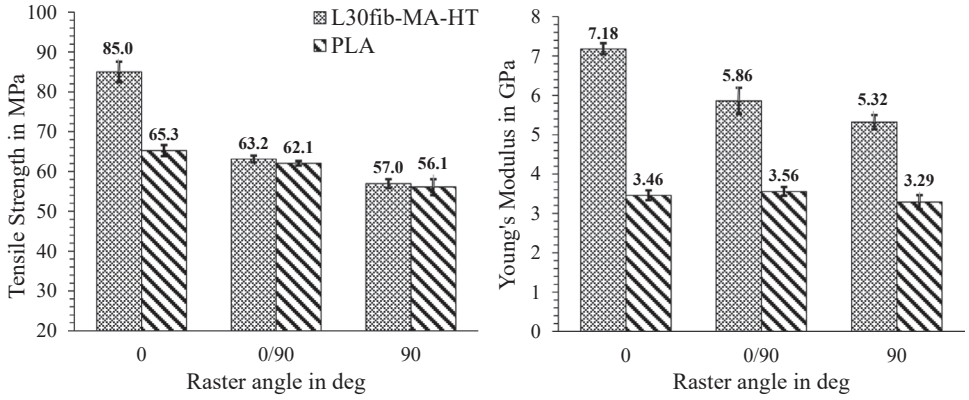

Fig. 13. Average tensile strength and Young's modulus of neat PLA and heat-treated L30fib-MA composites printed with different raster angle infill. The error bars indicate one standard deviation.

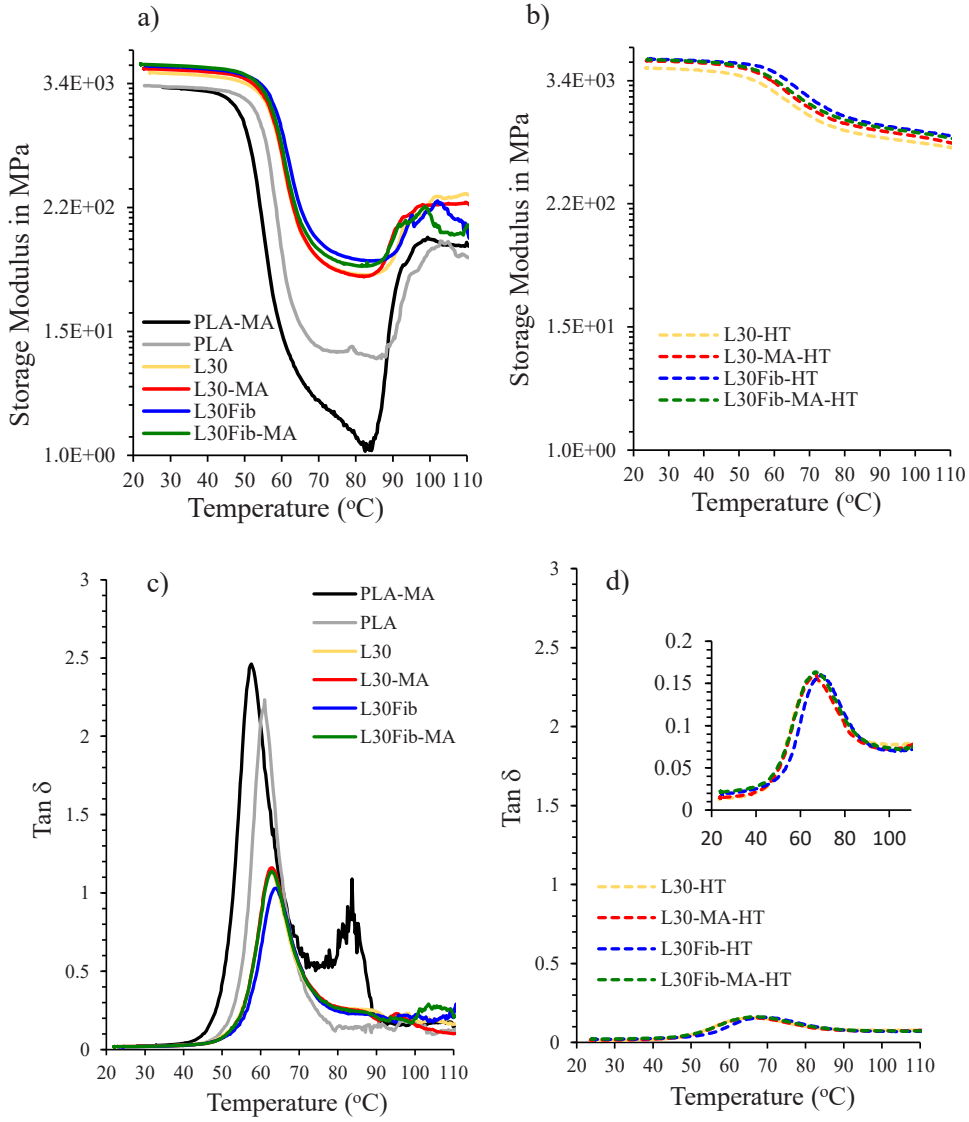

Fig. 14. Storage modulus and Tanδ curves of as-printed composites with 30 mass% of fibre and neat PLA (a, c) and the heat-treated composites (b,d).

mobility of PLA molecules, resulting in higher storage modulus at higher temperatures. The heat treatment of the composite samples for DMA was conducted with the tensile test samples at 105 °C, which is close to the onset temperature for cold crystallisation. As shown in Tables 4 and 5, this temperature was enough to increase the crystallinity of PLA to around 30%. The post-printing heat treatment had a significant influence on the thermo-mechanical behaviour of the composites. The heat-treated composite samples had an improvement in E' of a few orders of

magnitude above approximately 60 °C (Fig. 14b). Table 7 shows that, even at 60 °C, the modified formulations (L30-MA, L30Fib, and L30Fib-MA) have E' at 60 °C higher than neat PLA at 25 °C. At 80 °C, the heat-treated L30Fib sample has an E' 200 times higher than neat PLA at the same temperature, and the L30Fib-MA sample has an E' 1100 times higher than the PLA-MA sample. The effect of heat treatment is also observed in the sharp decrease in the max tanδ values (Fig. 14d) and increase in the tanδ peak temperatures (see Table 7), which indicates a predominance of elastic behaviour instead of rubbery behaviour.

Changes in the interfacial bonding between fibre and matrix can also be verified by DMA. The effectiveness coefficient (C) is calculated using the storage modulus of neat polymer (matrix) and composite in the glassy and rubbery regions according to Eq. (6) [97]. The adhesion factor (A) is calculated with the maximum values of tanδ of the neat polymer and composite using Eq. (7) [98].

$$C = \frac{\frac{E_g^{'}}{E_r^{'}}(composite)}{\frac{E_g^{'}}{E_r^{'}}(neat \quad PLA)} \tag{6}$$

$$A = \frac{1}{(1 - L_f)} \frac{\tan\delta_c}{\tan\delta_p} - 1 \tag{7}$$

Where C is the effectiveness coefficient, $E_g^{'}$ is the storage modulus in the glassy region (25 °C), $E_r^{'}$ is the storage modulus in the rubbery region (80 °C), L_f is the mass fraction of fibres, $\tan\delta_c$ is the maximum tanδ of the composite, and $\tan\delta_p$ is the maximum tanδ of neat PLA (or PLA-MA).

With the increase in the interfacial adhesion between fibre and matrix, there is a reduction in the molecular mobility around the fibres. Therefore, lower values of adhesion factor and effectiveness coefficient generally indicate better fibre/matrix interfacial bonding [4,44,97,98]. Table 8 summarises the effectiveness coefficient and adhesion factor of the formulations with 30 mass% of lyocell fibres. The values used to calculate both parameters are also included in Table 8. For the formulations using MA, the values of PLA-MA were used and for the formulations based on PLA only, the PLA condition was used. It is evident that the modifications used in this study, both the addition of MA and fibrillation of fibres, improved the interface and compatibility between fibre and matrix. The L30Fib sample, for example, presented lower values of A and C than the composite with unmodified fibres (L30), which demonstrates that the increased roughness of the fibres and the mechanical anchoring of the fibres by the nanofibrils improved the adhesion between the lyocell fibres and the matrix. Although the samples modified with MA had lower E' at 80 °C than the unmodified counterparts, the lower values of A and C show that the modification with MA successfully improved the fibre/matrix adhesion. The lowest values of A and C were obtained by the sample modified with MA and reinforced with the fibrillated fibres (L30Fib-MA), which was also the condition that presented the best tensile properties. These results demonstrate that the combined modification of the fibre and matrix effectively improved the interfacial bonding between the lyocell fibres and PLA. Considering that the fibres in the composites are very short (approximately 125 μm), this improvement was fundamental to achieving the interesting mechanical properties reported in this work.

Table 7
Summary of DMA results obtained for 3D printed PLA and composites with 30 mass% of lyocell fibre.

Condition	E'* at 25 °C in MPa	E'* at 60 °C in MPa	E'* 80 °C in MPa	Max. tanδ	Max. tanδ temperature in °C
As-printed					
PLA	3214	96.62	7.680	2.233	61.0
PLA-MA	3053	16.23	1.293	2.607	58.1
L30	4289	729.0	52.58	1.133	62.8
L30-MA	4645	785.6	50.90	1.161	63.0
L30Fib	4954	1291	72.71	1.032	63.9
L30Fib-MA	5099	907.7	63.13	1.137	62.8
Heat-treated					
L30	4451	2643	1134	0.157	66.8
L30-MA	5209	3276	1322	0.160	67.2
L30Fib	5409	4102	1541	0.160	69.2
L30Fib-MA	5347	3461	1424	0.164	67.0

* E' = Storage modulus.

Table 8
Storage modulus E' at 25 °C and 80 °C, effectiveness coefficient (C), max. tanδ and adhesion factor (A) for the PLA composites with 30 mass% of lyocell fibres.

Condition	E'at 25 °C in MPa	E' 80 °C in MPa	Effectiveness coefficient (C)	Max. tanδ	Adhesion factor (A)
As-printed					
PLA	3214	7.680	1	2.233	0
PLA-MA	3053	1.293	1	2.607	0
L30	4289	52.58	0.256	1.133	-0.276
L30-MA	4645	50.90	0.039	1.161	-0.364
L30Fib	4954	72.71	0.213	1.032	-0.340
L30Fib-MA	5099	63.13	0.034	1.137	-0.377

4. Conclusions

The use of renewable resources for the production of materials is paramount to improving the sustainability of additive manufacturing processes. However, mechanical performance is often sacrificed by the use of materials with lower environmental impact. In this work, 3D printable composites reinforced with short lyocell fibres with remarkable mechanical properties were developed. The use of fibre fibrillation and matrix modification were fundamental in improving the load transfer between fibre and matrix, which was proved by mechanical testing and dynamic mechanical analysis.

By modifying PLA with MA, it was possible to increase the composites' tensile strength and Young's modulus with the addition of lyocell fibres. The composite with 30 mass% of fibres showed an improvement of 23% in tensile strength and 79% in Young's modulus in comparison with the modified PLA. Although the addition of MA and DCP may have caused a reduction in the PLA's molecular mass, the resulting decrease of viscosity during compounding and possible grafting of MA into PLA improved the fibre/matrix adhesion and, consequently, the mechanical properties of the composites.

The lyocell fibres were also submitted to a fibrillation process. Nanofibrils between 100 and 300 nm and increased surface roughness were observed on the modified fibres. These features resulted in better anchoring of the fibres into the matrix comparable to the rooting of plants in the soil. The best tensile properties results were obtained by using the fibrillated lyocell fibres in combination with PLA modified with MA; an improvement of 31.2% in tensile strength and 27.5% in Young's modulus in comparison with the formulation with unmodified fibre and PLA.

The use of post-printing heat treatment was also beneficial in enhancing the mechanical properties of all the composite formulations. It is hypothesised that this effect was attributed to the increase in PLA's crystallinity and better fibre/matrix interface. The best properties were achieved by the formulation with 30 mass% of fibrillated fibres in the PLA-MA matrix. After heat treatment, this sample showed a tensile strength of 85 MPa and Young's modulus of 7.18 GPa while maintaining a strain at break of 3.19%. The increase in the crystallinity of PLA also resulted in a considerable improvement in the thermo-mechanical stability of the composites with 30 mass% of fibres, considerably increasing the storage modulus at higher temperatures; at 80 °C, the E' was 200 times higher in comparison with neat PLA and 1100 times higher than

PLA modified with MA.

There are many technical advantages of using 3D printing methods to process cellulose fibre-reinforced composites. Through the development of this work, we have shown that with a proper interface between fibre and matrix and with fibre alignment induced by 3D printing, very promising mechanical properties can be achieved, even if very short fibres are used. With freedom of design enabled by 3D printing and the selective deposition of a composite with aligned fibres, objects with variable stiffness and functionally graded properties can be realised.

CRediT authorship contribution statement

Kim L. Pickering: Writing – review & editing, Resources, Funding acquisition, Conceptualization. **Christian Gauss:** Writing – original draft, Methodology, Investigation, Formal analysis, Conceptualization. **Nina Graupner:** Writing – review & editing, Investigation, Formal analysis, Conceptualization. **Jörg Müssig:** Writing – review & editing, Resources, Conceptualization.

Declaration of Competing Interest

The authors declare that they have no known competing financial interests or personal relationships that could have appeared to influence the work reported in this paper.

Data availability

Data will be made available on request.

Acknowledgements

The authors would like to thank the financial support from the Ministry of Business, Innovation and Employment of New Zealand through the National Science Challenge spearhead project “Additive manufacturing and 3D and/or 4D printing of bio-composites” [grant 2019-S5-CRS] and the MBIE New Zealand Endeavour Fund, through the project Āmiomio Aotearoa – A circular Economy for the wellbeing of New Zealand (UOWX2004).

Appendix A. Supporting information

Supplementary data associated with this article can be found in the online version at doi:10.1016/j.addma.2023.103806.

References

[1] K.L. Pickering, M.G.A. Efendy, T.M. Le, A review of recent developments in natural fibre composites and their mechanical performance, Compos. Part A Appl. Sci. Manuf. 83 (2016) 98–112, https://doi.org/10.1016/j.compositesa.2015.08.038.
[2] M.P. Ho, K.T. Lau, H. Wang, D. Hui, Improvement on the properties of polylactic acid (PLA) using bamboo charcoal particles, Compos. Part B Eng. 81 (2015) 14–25, https://doi.org/10.1016/j.compositesb.2015.05.048.
[3] M. Feldmann, A.K. Bledzki, Bio-based polyamides reinforced with cellulosic fibres - processing and properties, Compos. Sci. Technol. 100 (2014) 113–120, https://doi.org/10.1016/j.compscitech.2014.06.008.
[4] J.O. Akindoyo, K. Pickering, M.D. Beg, M. Mucalo, Combined digestion and bleaching of New Zealand flax /harakeke fibre and its effects on the mechanical, thermal, and dynamic mechanical properties of poly(lactic) acid matrix composites, Compos. Part A Appl. Sci. Manuf. 164 (2023), 107326, https://doi.org/10.1016/j.compositesa.2022.107326.
[5] N. Graupner, Application of lignin as natural adhesion promoter in cotton fibre-reinforced poly(lactic acid) (PLA) composites, J. Mater. Sci. 43 (2008) 5222–5229, https://doi.org/10.1007/s10853-008-2762-3.
[6] T. Sunny, K.L. Pickering, J. McDonald-Wharry, Improving the alignment of dynamic sheet-formed mats by changing nozzle geometry and their reinforcement of polypropylene matrix composites, J. Compos. Sci. 5 (2021), https://doi.org/10.3390/jcs5090226.
[7] B. Baghaei, M. Skrifvars, M. Rissanen, S.K. Ramamoorthy, Mechanical and thermal characterization of compression moulded polylactic acid natural fiber composites reinforced with hemp and lyocell fibers, J. Appl. Polym. Sci. 131 (2014) 1–10, https://doi.org/10.1002/app.40534.
[8] L.P. Muthe, K. Pickering, C. Gauss, A review of 3D/4D printing of poly-lactic acid composites with bio-derived reinforcements, Compos. Part C. Open Access 8 (2022), 100271, https://doi.org/10.1016/j.jcomc.2022.100271.
[9] M.D.H. Beg, K.L. Pickering, C. Gauss, The effects of alkaline digestion, bleaching and ultrasonication treatment of fibre on 3D printed harakeke fibre reinforced polylactic acid composites, Compos. Part A Appl. Sci. Manuf. 166 (2023), 107384, https://doi.org/10.1016/j.compositesa.2022.107384.
[10] C. Gauss, K.L. Pickering, J. Tshuma, J. McDonald-Wharry, Production and assessment of poly(lactic acid) matrix composites reinforced with regenerated cellulose fibres for fused deposition modelling, Polymers 14 (2022) 3991, https://doi.org/10.3390/polym14193991.
[11] A. Le Duigou, A. Barbé, E. Guillou, M. Castro, 3D printing of continuous flax fibre reinforced biocomposites for structural applications, Mater. Des. 180 (2019), 107884, https://doi.org/10.1016/j.matdes.2019.107884.
[12] C. Gauss, K. Pickering, L.P. Muthe, The use of cellulose in bio-derived formulations for 3D/4D printing: a review, Compos. Part C Open Access 4 (2021), 100113, https://doi.org/10.1016/j.jcomc.2021.100113.
[13] X. Xiao, V.S. Chevali, P. Song, D. He, H. Wang, Polylactide/hemp hurd biocomposites as sustainable 3D printing feedstock, Compos. Sci. Technol. 184 (2019), 107887, https://doi.org/10.1016/j.compscitech.2019.107887.
[14] M.G.A. Efendy, K.L. Pickering, Fibre orientation of novel dynamically sheet formed discontinuous natural fibre PLA composites, Compos. Part A Appl. Sci. Manuf. 90 (2016) 82–89, https://doi.org/10.1016/j.compositesa.2016.07.003.
[15] T. Lu, S. Liu, M. Jiang, X. Xu, Y. Wang, Z. Wang, J. Gou, D. Hui, Z. Zhou, Effects of modifications of bamboo cellulose fibers on the improved mechanical properties of cellulose reinforced poly(lactic acid) composites, Compos. Part B Eng. 62 (2014) 191–197, https://doi.org/10.1016/j.compositesb.2014.02.030.
[16] H.L. Tekinalp, X. Meng, Y. Lu, V. Kunc, L.J. Love, W.H. Peter, S. Ozcan, High modulus biocomposites via additive manufacturing: cellulose nanofibril networks as “microsponges”, Compos. Part B Eng. 173 (2019), 106817 https://doi.org/10.1016/j.compositesb.2019.05.028.
[17] J. Taylor, Controlling fibrillation - experiences of the dyeing and finishing of lyocell fibres, Color. Technol. 131 (2015) 424–433, https://doi.org/10.1111/cote.12184.
[18] J. Ganster, H.P. Fink, Novel cellulose fibre reinforced thermoplastic materials, Cellulose 13 (2006) 271–280, https://doi.org/10.1007/s10570-005-9045-9.
[19] R.K. Johnson, A. Zink-Sharp, S.H. Renneckar, W.G. Glasser, Mechanical properties of wetlaid lyocell and hybrid fiber-reinforced composites with polypropylene, Compos. Part A Appl. Sci. Manuf. 39 (2008) 470–477, https://doi.org/10.1016/j.compositesa.2007.12.007.
[20] M. Cordin, T. Bechtold, T. Pham, Effect of fibre orientation on the mechanical properties of polypropylene–lyocell composites, Cellulose 25 (2018) 7197–7210, https://doi.org/10.1007/s10570-018-2079-6.
[21] Q. Cheng, S. Wang, T.G. Rials, S.H. Lee, Physical and mechanical properties of polyvinyl alcohol and polypropylene composite materials reinforced with fibril aggregates isolated from regenerated cellulose fibers, Cellulose 14 (2007) 593–602, https://doi.org/10.1007/s10570-007-9141-0.
[22] F. Carrillo, X. Colom, X. Cañavate, Properties of regenerated cellulose lyocell fiber-reinforced composites, J. Reinf. Plast. Compos 29 (2010) 359–371, https://doi.org/10.1177/0731684408097777.
[23] H. Zhang, Q. Li, K.J. Edgar, G. Yang, H. Shao, Structure and properties of flax vs. lyocell fiber-reinforced polylactide stereocomplex composites, Cellulose 28 (2021) 9297–9308, https://doi.org/10.1007/s10570-021-04105-0.
[24] N. Graupner, G. Ziegmann, F. Wilde, F. Beckmann, J. Müssig, Procedural influences on compression and injection moulded cellulose fibre-reinforced polylactide (PLA) composites: influence of fibre loading, fibre length, fibre orientation and voids, Compos. Part A Appl. Sci. Manuf. 81 (2016) 158–171, https://doi.org/10.1016/j.compositesa.2015.10.040.
[25] N.P.G. Suardana, A. Abdalla, H.K. Kim, K.S. Choi, J.K. Lim, Mechanical properties and biodegradability of green composites based on biodegradable polyesters and lyocell fabric, in: Proceedings of the ICCM International Conference on Composite Materials, 2011.
[26] M. Yu, H. Zhang, Z. Liu, Z. Ge, F. Kong, H. Shao, X. Hu, Effects of fiber dimension and its distribution on the properties of lyocell and ramie fibers reinforced polylactide composites, Fibers Polym. 20 (2019) 1726–1732, https://doi.org/10.1007/s12221-019-1171-3.
[27] M.A. Gunning, L.M. Geever, J.A. Killion, J.G. Lyons, C.L. Higginbotham, Mechanical and biodegradation performance of short natural fibre polyhydroxybutyrate composites, Polym. Test. 32 (2013) 1603–1611, https://doi.org/10.1016/j.polymertesting.2013.10.011.
[28] S. Zhang, C. Chen, C. Duan, H. Hu, H. Li, J. Li, Y. Liu, X. Ma, J. Stavik, Y. Ni, Regenerated cellulose by the lyocell process, a brief review of the process and properties, BioResources 13 (2018) 1–16, https://doi.org/10.15376/biores.13.2.Zhang.
[29] D. Klemm, B. Heublein, H.P. Fink, A. Bohn, Cellulose: fascinating biopolymer and sustainable raw material, Angew. Chem. Int. Ed. 44 (2005) 3358–3393, https://doi.org/10.1002/anie.200460587.
[30] P. Langan, Y. Nishiyama, H. Chanzy, X-ray structure of mercerized cellulose II at 1 Å resolution, Biomacromolecules 2 (2001) 410–416, https://doi.org/10.1021/bm005612q.
[31] R.J. Moon, A. Martini, J. Nairn, J. Simonsen, J. Youngblood, Cellulose nanomaterials review: structure, properties and nanocomposites, Chem. Soc. Rev. 40 (2011) 3941, https://doi.org/10.1039/c0cs00108b.
[32] C.G. Silva, D. Benaducci, E. Frollini, Lyocell and cotton fibers as reinforcements for a thermoset polymer, BioResources 7 (2012) 78–98, https://doi.org/10.15376/biores.7.1.0078-0098.

[33] S.K. Ramamoorthy, C.K. Kundu, K. Adekunle, T. Bashir, M. Skrifvars, Properties of green composites with regenerated cellulose fiber and soybean-based thermoset for technical applications, J. Reinf. Plast. Compos. 33 (2014) 193–201, https://doi.org/10.1177/0731684413504325.
[34] K. Adekunle, C. Patzelt, A. Kalantar, M. Skrifvars, Mechanical and viscoelastic properties of soybean oil thermoset reinforced with jute fabrics and carded lyocell fiber, J. Appl. Polym. Sci. 122 (2011) 2855–2863, https://doi.org/10.1002/app.34360.
[35] B.S. Kim, M.M. Kim, J.R. Ha, M.K. Um, B.H. Chun, Effect of plasma treatment on Lyocell fabric/PLA, WIT Trans. Built Environ. 112 (2010) 271–277, https://doi.org/10.2495/HPSM100251.
[36] T. Takahashi, K. Hirayama, N. Teramoto, M. Shibata, Biocomposites composed of epoxidized soybean oil cured with terpene-based acid anhydride and cellulose fibers, J. Appl. Polym. Sci. 108 (2008) 1596–1602, https://doi.org/10.1002/app.27866.
[37] Z.L. Yan, H. Wang, K.T. Lau, S. Pather, J.C. Zhang, G. Lin, Y. Ding, Reinforcement of polypropylene with hemp fibres, Compos. Part B Eng. 46 (2013) 221–226, https://doi.org/10.1016/j.compositesb.2012.09.027.
[38] N. Graupner, H. Fischer, G. Ziegmann, J. Müssig, Improvement and analysis of fibre/matrix adhesion of regenerated cellulose fibre reinforced PP-, MAPP- and PLA-composites by the use of Eucalyptus globulus lignin, Compos. Part B Eng. 66 (2014) 117–125, https://doi.org/10.1016/j.compositesb.2014.05.002.
[39] L. Petersson, K. Oksman, A.P. Mathew, Using maleic anhydride grafted poly(lactic acid) as a compatibilizer in poly(lactic acid)/layered-silicate nanocomposites, J. Appl. Polym. Sci. 102 (2006) 1852–1862, https://doi.org/10.1002/app.24121.
[40] S. Chauhan, N. Raghu, A. Raj, Effect of maleic anhydride grafted polylactic acid concentration on mechanical and thermal properties of thermoplasticized starch filled polylactic acid blends, Polym. Polym. Compos. 29 (2021) S400–S410, https://doi.org/10.1177/09673911211004194.
[41] S.W. Hwang, S.B. Lee, C.K. Lee, J.Y. Lee, J.K. Shim, S.E.M. Selke, H. Soto-Valdez, L. Matuana, M. Rubino, R. Auras, Grafting of maleic anhydride on poly(L-lactic acid). Effects on physical and mechanical properties, Polym. Test. 31 (2012) 333–344, https://doi.org/10.1016/j.polymertesting.2011.12.005.
[42] S.K. Ramamoorthy, M. Skrifvars, M. Rissanen, Effect of alkali and silane surface treatments on regenerated cellulose fibre type (Lyocell) intended for composites, Cellulose 22 (2015) 637–654, https://doi.org/10.1007/s10570-014-0526-6.
[43] M.A. Sawpan, K.L. Pickering, A. Fernyhough, Flexural properties of hemp fibre reinforced polylactide and unsaturated polyester composites, Compos. Part A Appl. Sci. Manuf. 43 (2012) 519–526, https://doi.org/10.1016/j.compositesa.2011.11.021.
[44] C. Gauss, K.L. Pickering, A new method for producing polylactic acid biocomposites for 3D printing with improved tensile and thermo-mechanical performance using grafted nanofibrillated cellulose, Addit. Manuf. 61 (2023), 103346, https://doi.org/10.1016/j.addma.2022.103346.
[45] N. Graupner, K. Albrecht, D. Hegemann, J. Müssig, Plasma modification of man-made cellulose fibers (Lyocell) for improved fiber/matrix adhesion in poly(lactic acid) composites, J. Appl. Polym. Sci. 128 (2013) 4378–4386, https://doi.org/10.1002/app.38663.
[46] J.O. Karlsson, J.F. Blachot, A. Peguy, P. Gatenholm, Improvement of adhesion between polyethylene and regenerated cellulose fibers by surface fibrillation, Polym. Compos. 17 (1996) 300–304, https://doi.org/10.1002/pc.10614.
[47] N. Graupner, S. Schmidt, C. Gauss, J. Müssig, Making positive use of the fibrillation of lyocell fibres in composite materials, Compos. Part C Open Access 11 (2023), 100359, https://doi.org/10.1016/j.jcomc.2023.100359.
[48] N. Graupner, S. Schmidt, C. Gauss, J. Müssig, Making positive use of the fibrillation of lyocell fibres in composite materials, Compos. Part C Open Access (2023), 100359, https://doi.org/10.1016/j.jcomc.2023.100359.
[49] K. Moriam, D. Sawada, K. Nieminen, M. Hummel, Y. Ma, M. Rissanen, H. Sixta, Towards regenerated cellulose fibers with high toughness, Cellulose 28 (2021) 9547–9566, https://doi.org/10.1007/s10570-021-04134-9.
[50] W. Zhang, S. Okubayashi, T. Bechtold, Fibrillation tendency of cellulosic fibers. Part 1: effects of swelling, Cellulose 12 (2005) 267–273, https://doi.org/10.1007/s10570-004-2786-z.
[51] P. Parajuli, S. Acharya, S.S. Rumi, M.T. Hossain, N. Abidi, Regenerated cellulose in textiles: rayon, lyocell, modal and other fibres, in: Fundamentals of Natural Fibres and Textiles, Elsevier, 2021, pp. 87–110, https://doi.org/10.1016/B978-0-12-821483-1.00015-2.
[52] X. Zhao, H. Tekinalp, X. Meng, D. Ker, B. Benson, Y. Pu, A.J. Ragauskas, Y. Wang, K. Li, E. Webb, D.J. Gardner, J. Anderson, S. Ozcan, Poplar as biofiber reinforcement in composites for large-scale 3D printing, ACS Appl. Bio Mater. (2019), https://doi.org/10.1021/acsabm.9b00675.
[53] K.E. Mazur, A. Borucka, P. Kaczor, S. Gądek, R. Bogucki, D. Mirzewiński, S. Kuciel, Mechanical, thermal and microstructural characteristic of 3D printed polylactide composites with natural fibers: wood, bamboo and cork, J. Polym. Environ. 30 (2022) 2341–2354, https://doi.org/10.1007/s10924-021-02356-3.
[54] J. Arnold, D.A. Smith, 3D printed polylactic acid - hemp fiber composites: mechanical, thermal, and microcomputed tomography data, Data Brief 39 (2021), 107534, https://doi.org/10.1016/j.dib.2021.107534.
[55] C. Badouard, F. Traon, C. Denoual, C. Mayer-Laigle, G. Paës, A. Bourmaud, Exploring mechanical properties of fully compostable flax reinforced composite filaments for 3D printing applications, Ind. Crop. Prod. 135 (2019) 246–250, https://doi.org/10.1016/j.indcrop.2019.04.049.
[56] D. Filgueira, S. Holmen, J.K. Melbø, D. Moldes, A.T. Echtermeyer, G. Chinga-Carrasco, Enzymatic-assisted modification of thermomechanical pulp fibers to improve the interfacial adhesion with poly(lactic acid) for 3D printing, ACS Sustain. Chem. Eng. 5 (2017) 9338–9346, https://doi.org/10.1021/acssuschemeng.7b02351.
[57] J. Dong, C. Mei, J. Han, S. Lee, Q. Wu, 3D printed poly(lactic acid) composites with grafted cellulose nanofibers: Effect of nanofiber and post-fabrication annealing treatment on composite flexural properties, Addit. Manuf. 28 (2019) 621–628, https://doi.org/10.1016/j.addma.2019.06.004.
[58] B. Wang, T. Wen, X. Zhang, A. Tercjak, X. Dong, A.J. Müller, D. Wang, D. Cavallo, Nucleation of poly(lactide) on the surface of different fibers, Macromolecules 52 (2019) 6274–6284, https://doi.org/10.1021/acs.macromol.9b01078.
[59] S. Bhandari, R.A. Lopez-Anido, D.J. Gardner, Enhancing the interlayer tensile strength of 3D printed short carbon fiber reinforced PETG and PLA composites via annealing, Addit. Manuf. 30 (2019), 100922, https://doi.org/10.1016/j.addma.2019.100922.
[60] N. Graupner, Improvement of the mechanical properties of biodegradable hemp fiber reinforced poly(lactic acid) (PLA) composites by the admixture of man-made cellulose fibers, J. Compos. Mater. 43 (2009) 689–702, https://doi.org/10.1177/0021998308100688.
[61] N. Graupner, J. Müssig, A comparison of the mechanical characteristics of kenaf and lyocell fibre reinforced poly(lactic acid) (PLA) and poly(3-hydroxybutyrate) (PHB) composites, Compos. Part A Appl. Sci. Manuf. 42 (2011) 2010–2019, https://doi.org/10.1016/j.compositesa.2011.09.007.
[62] B. Baghaei, M. Skrifvars, Characterisation of polylactic acid biocomposites made from prepregs composed of woven polylactic acid/hemp-Lyocell hybrid yarn fabrics, Compos. Part A Appl. Sci. Manuf. 81 (2016) 139–144, https://doi.org/10.1016/j.compositesa.2015.10.042.
[63] N. Graupner, G. Ziegmann, J. Müssig, Composite models for compression moulded long regenerated cellulose fibre-reinforced brittle polylactide (PLA), Compos. Sci. Technol. 149 (2017) 55–63, https://doi.org/10.1016/j.compscitech.2017.05.028.
[64] N. Graupner, A.S. Herrmann, J. Müssig, Natural and man-made cellulose fibre-reinforced poly(lactic acid) (PLA) composites: an overview about mechanical characteristics and application areas, Compos. Part A Appl. Sci. Manuf. 40 (2009) 810–821, https://doi.org/10.1016/j.compositesa.2009.04.003.
[65] N. Graupner, J. Müssig, Cellulose fiber-reinforced PLA versus PP, Int. J. Polym. Sci. (2017) (2017), https://doi.org/10.1155/2017/6059183.
[66] N. Graupner, K. Albrecht, G. Ziegmann, H. Enzler, J. Müssig, Influence of reprocessing on fibre length distribution, tensile strength and impact strength of injection moulded cellulose fibre-reinforced polylactide (PLA) composites, Express Polym. Lett. 10 (2016) 647–663, https://doi.org/10.3144/expresspolymlett.2016.59.
[67] S. Pilla, S. Gong, E. O'Neill, R.M. Rowell, A.M. Krzysik, Polylactide-pine wood flour composites, Polym. Eng. Sci. 48 (2008) 578–587, https://doi.org/10.1002/pen.20971.
[68] N. Graupner, Analyse und Optimierung der Struktur- und Eigenschaftsbeziehungen von cellulosefaserverstärkten Polylactid-Verbundwerkstoffen, Papierflieger Verlag, Clausthal-Zellerfeld, 2014.
[69] L. Zhou, H. He, M. chun Li, S. Huang, C. Mei, Q. Wu, Enhancing mechanical properties of poly(lactic acid) through its in-situ crosslinking with maleic anhydride-modified cellulose nanocrystals from cottonseed hulls, Ind. Crop. Prod. 112 (2018) 449–459, https://doi.org/10.1016/j.indcrop.2017.12.044.
[70] H. Oliver-Ortega, R. Reixach, F.X. Espinach, J.A. Méndez, Maleic anhydride polylactic acid coupling agent prepared from solvent reaction: synthesis, characterization and composite performance, Materials 15 (2022), https://doi.org/10.3390/ma15031161.
[71] T. Tábi, S. Hajba, J.G. Kovács, Effect of crystalline forms (α′ and α) of poly(lactic acid) on its mechanical, thermo-mechanical, heat deflection temperature and creep properties, Eur. Polym. J. 82 (2016) 232–243, https://doi.org/10.1016/j.eurpolymj.2016.07.024.
[72] J. Dong, M. Li, L. Zhou, S. Lee, C. Mei, X. Xu, Q. Wu, The influence of grafted cellulose nanofibers and postextrusion annealing treatment on selected properties of poly(lactic acid) filaments for 3D printing, J. Polym. Sci. Part B Polym. Phys. 55 (2017) 847–855, https://doi.org/10.1002/polb.24333.
[73] H. Liu, H. He, X. Peng, B. Huang, J. Li, Three-dimensional printing of poly(lactic acid) bio-based composites with sugarcane bagasse fiber: effect of printing orientation on tensile performance, Polym. Adv. Technol. 30 (2019) 910–922, https://doi.org/10.1002/pat.4524.
[74] L. Jiang, T. Shen, P. Xu, X. Zhao, X. Li, W. Dong, P. Ma, M. Chen, Crystallization modification of poly(lactide) by using nucleating agents and stereocomplexation, E-Polymers 16 (2016) 1–13, https://doi.org/10.1515/epoly-2015-0179.
[75] B. Coppola, N. Cappetti, L. Di Maio, P. Scarfato, L. Incarnato, 3D printing of PLA/clay nanocomposites: influence of printing temperature on printed samples properties, Materials 11 (2018), https://doi.org/10.3390/ma11101947.
[76] S. Tanpichai, W.W. Sampson, S.J. Eichhorn, Stress transfer in microfibrillated cellulose reinforced poly(vinyl alcohol) composites, Compos. Part A Appl. Sci. Manuf. 65 (2014) 186–191, https://doi.org/10.1016/j.compositesa.2014.06.014.
[77] A. Giubilini, G. Siqueira, F.J. Clemens, C. Sciancalepore, M. Messori, G. Nystrom, F. Bondioli, 3D printing nanocellulose-poly(3-hydroxybutyrate-co-3-hydroxyhexanoate) biodegradable composites by fused deposition modeling, ACS Sustain. Chem. Eng. (2020), https://doi.org/10.1021/acssuschemeng.0c03385.
[78] A.D. French, Idealized powder diffraction patterns for cellulose polymorphs, Cellulose 21 (2014) 885–896, https://doi.org/10.1007/s10570-013-0030-4.
[79] N. Yoshiharu, K. Shigenori, W. Masahisa, O. Takeshi, Cellulose microcrystal film of high uniaxial orientation, Macromolecules 30 (1997) 6395–6397, https://doi.org/10.1021/ma970503y.
[80] D.K.K. Cavalcanti, J.S.S. Neto, H.F.M. d Queiroz, Y. Wu, V.F.S. Neto, M.D. Banea, Development and mechanical characterization of short curauá fiber-reinforced PLA

composites made via fused deposition modeling, Polymers 14 (2022), https://doi.org/10.3390/polym14225047.
[81] J. Yan, E. Demirci, A. Gleadall, Are classical fibre composite models appropriate for material extrusion additive manufacturing? A thorough evaluation of analytical models, SSRN Electron. J. 62 (2022), 103371, https://doi.org/10.2139/ssrn.4110391.
[82] E.M. Agaliotis, B.D. Ake-Concha, A. May-Pat, J.P. Morales-Arias, C. Bernal, A. Valadez-Gonzalez, P.J. Herrera-Franco, G. Proust, J.F. Koh-Dzul, J.G. Carrillo, E. A. Flores-Johnson, Tensile behavior of 3D printed polylactic acid (PLA) based composites reinforced with natural fiber, Polymers 14 (2022), https://doi.org/10.3390/polym14193976.
[83] N. Giani, L. Mazzocchetti, T. Benelli, F. Picchioni, L. Giorgini, Towards sustainability in 3D printing of thermoplastic composites: Evaluation of recycled carbon fibers as reinforcing agent for FDM filament production and 3D printing, Compos. Part A Appl. Sci. Manuf. 159 (2022), https://doi.org/10.1016/j.compositesa.2022.107002.
[84] S. Al Zahmi, S. Alhammadi, A. Elhassan, W. Ahmed, Carbon fiber/PLA recycled composite, Polymers 14 (2022), https://doi.org/10.3390/polym14112194.
[85] E.O. Cisneros-López, A.K. Pal, A.U. Rodriguez, F. Wu, M. Misra, D.F. Mielewski, A. Kiziltas, A.K. Mohanty, Recycled poly(lactic acid)–based 3D printed sustainable biocomposites: a comparative study with injection molding, Mater. Today Sustain. 7–8 (2020) 1–12, https://doi.org/10.1016/j.mtsust.2019.100027.
[86] D. Stoof, K. Pickering, Y. Zhang, Fused deposition modelling of natural fibre/polylactic acid composites, J. Compos. Sci. 1 (2017) 8, https://doi.org/10.3390/jcs1010008.
[87] L. Sang, S. Han, Z. Li, X. Yang, W. Hou, Development of short basalt fiber reinforced polylactide composites and their feasible evaluation for 3D printing applications, Compos. Part B Eng. 164 (2019) 629–639, https://doi.org/10.1016/j.compositesb.2019.01.085.
[88] N. Maqsood, M. Rimašauskas, Characterization of carbon fiber reinforced PLA composites manufactured by fused deposition modeling, Compos. Part C Open Access (2021), 100112, https://doi.org/10.1016/j.jcomc.2021.100112.
[89] Z. Liu, Q. Lei, S. Xing, Mechanical characteristics of wood, ceramic, metal and carbon fiber-based PLA composites fabricated by FDM, J. Mater. Res. Technol. 8 (2019) 3743–3753, https://doi.org/10.1016/j.jmrt.2019.06.034.
[90] B.M. Tymrak, M. Kreiger, J.M. Pearce, Mechanical properties of components fabricated with open-source 3-D printers under realistic environmental conditions, Mater. Des. 58 (2014) 242–246, https://doi.org/10.1016/j.matdes.2014.02.038.
[91] M. Caminero, J. Chacón, E. García-Plaza, P. Núñez, J. Reverte, J. Becar, Additive manufacturing of PLA-based composites using fused filament fabrication: effect of graphene nanoplatelet reinforcement on mechanical properties, dimensional accuracy and texture, Polymers 11 (2019) 799, https://doi.org/10.3390/polym11050799.
[92] S. Landes, T. Letcher, Mechanical strength of bamboo filled pla composite material in fused filament fabrication, J. Compos. Sci. 4 (2020), https://doi.org/10.3390/jcs4040159.
[93] CarbonXTM CF-PLA 3D Printing Filament, (n.d.). ⟨https://www.3dxtech.com/product/carbonx-pla-cf/⟩.
[94] Wood-Filled PLA 1.75mm Light Brown 1KG, (n.d.). ⟨https://www.imaginplastics.co.nz/shop/3D+Printing+Filament/PLA+Polylactic+acid/PLA%3A+Wood-Filled/Wood-Filled+PLA+1.75mm/Wood-Filled+PLA+1.75mm+Light+Brown+1KG-1001%3Fsku=1001.html⟩.
[95] N. Maqsood, M. Rimašauskas, Characterization of carbon fiber reinforced PLA composites manufactured by fused deposition modeling, Compos. Part C Open Access 4 (2021), https://doi.org/10.1016/j.jcomc.2021.100112.
[96] G. Rajeshkumar, S. Arvindh Seshadri, G.L. Devnani, M.R. Sanjay, S. Siengchin, J. Prakash Maran, N.A. Al-Dhabi, P. Karuppiah, V.A. Mariadhas, N. Sivarajasekar, A. Ronaldo Anuf, Environment friendly, renewable and sustainable poly lactic acid (PLA) based natural fiber reinforced composites – a comprehensive review, J. Clean. Prod. 310 (2021), 127483, https://doi.org/10.1016/j.jclepro.2021.127483.
[97] D. Romanzini, A. Lavoratti, H.L. Ornaghi, S.C. Amico, A.J. Zattera, Influence of fiber content on the mechanical and dynamic mechanical properties of glass/ramie polymer composites, Mater. Des. 47 (2013) 9–15, https://doi.org/10.1016/j.matdes.2012.12.029.
[98] C.A. Correa, C.A. Razzino, E. Hage, Role of maleated coupling agents on the interface adhesion of polypropylene-wood composites, J. Thermoplast. Compos. Mater. 20 (2007) 323–339, https://doi.org/10.1177/0892705707078896.